Nonequilibrium theory of scanning tunneling spectroscopy via adsorbate resonances: Nonmagnetic and Kondo impurities

M. Plihal and J. W. Gadzuk
National Institute of Standards and Technology, Gaithersburg, Maryland 20899
(Received 5 June 2000; revised manuscript received 22 September 2000; published 1 February 2001)

We report on a fully nonequilibrium theory of scanning tunneling microscopy (STM) through resonances induced by impurity atoms adsorbed on metal surfaces. The theory takes into account the effect of tunneling current and finite bias on the system, and is valid for arbitrary intra-adsorbate electron correlation strength. It is thus applicable to recent STM experiments on Kondo impurities. We discuss the finite-temperature effects and the consequences of atomic scale resolution of the STM for the spectral property of such systems. We find that the tip position affects the resonance line shapes in two ways. As a function of the distance from the surface, the line shapes vary due to the different extents of the adsorbate and metal wave functions into the vacuum. However, we do not expect large variations in line shapes unless tunneling into the tightly bound adsorbate states is considerable, or nonequilibrium effects are significant. As a function of the lateral tip position, line shapes should not change significantly on length scales of $R_{\|} \leqslant 10$ Å under typical experimental conditions when the electrons tunnel into the perturbed bulk conduction states hybridized with the outer shell sp adsorbate orbitals. Tunneling into surfaces states on (111) surfaces of noble metals should be important for an observation of resonance at larger distances (>10 Å), and oscillatory variations in the line shape should develop. This long-range behavior was not resolved in recent experiments with Kondo impurities. The temperature dependence of the Kondo resonance cannot be deduced directly from the differential conductance, as the thermal broadening of the tip Fermi surface produces qualitatively similar effects of comparable and larger magnitudes. A careful deconvolution is necessary to extract the temperature dependence of the Kondo resonance. The finite-bias current-induced nonequilibrium effects in tunneling through Kondo impurities should produce a characteristic broadening of the resonance in the case of strong hybridization of the discrete state with the STM tip.

DOI: 10.1103/PhysRevB.63.085404 PACS number(s): 68.37.Ef, 72.10.Fk

I. INTRODUCTION

A considerable body of experience and wisdom within the area of solid-state tunneling phenomenon was built up throughout tunneling's ''golden era of the sixties.'' It was during this period that many of the defining fundamental ideas, basic theoretical strategies and methodologies, and broad scope of applications for tunnel structures were first realized. A general introduction to many of these achievements can be found in a number of comprehensive volumes,[1–3] and in the Nobel lectures of Esaki, Giaver, and Josephson, who were awarded the 1973 Nobel Prize in Physics for ''their (independent) discoveries regarding tunneling phenomena in solids.'' [4] It is against this background that astounding achievements in contemporary tunneling studies utilizing the single-atom spatial resolution of the scanning tunneling microscope (STM) are most meaningfully considered.[5–10] One phenomenon of key interest here which was first considered in the ''golden era'' is that of impurity/adsorbate-assisted elastic tunneling. Two bodies of work are particularly relevant to the present study. The first is the recognition by Appelbaum *et al.* of the possible role of the Kondo effect[11–13] in determining certain current-voltage characteristics (e.g., ''zero-bias anomalies'') of metal-oxide-metal tunnel junctions containing localized paramagnetic impurity states near the metal-oxide interfaces.[14] Second are the resonance tunneling studies involving valence electronic levels of single atoms adsorbed on metal surfaces, as probed in a field emission microscope configured for energy analysis (thus enabling electron spectroscopy) of the field-emitted electrons.[15–17] Many years later, useful parallels between the theory of single atom-resonance tunneling developed in the ''golden era'' and the theory of the STM, in the single-atom-tip limit, were unambiguously established.[18] Further discussion of these issues from the past will be offered throughout the text, when appropriate.

The basis for continuing interest and excitement in impurity/adsorbate-assisted tunneling is that the transparency of tunnel junctions can be dramatically enhanced by the presence of states localized within the barrier when they are in resonance with the tunneling electrons. Tunneling through such states is, for example, the origin of the conductance fluctuations quantum dots exhibit in the Coulomb blockade.[19] The tunneling probability in the presence of a ''barrier'' state is proportional to the spectral density produced by the hybridization of a localized state with the conduction electrons, and in many situations the current is given by the Breit-Wigner formula

$$I \propto \frac{\Gamma^2}{(\omega-\epsilon_0)^2+(\Gamma/2)^2}. \tag{1.1}$$

Here Γ is the width of the resonance produced by the hybridization with the conduction electrons in the right and left leads, and ϵ_0 is the energy of the local state. The value of Γ depends on the height and width of the barrier potential between the central region and the leads.

Recently, enhancements in the zero-bias conductance in quantum dots due to the Kondo effect have been observed.[20] It was shown earlier that (dI/dV), the zero-bias differential conductance, is proportional to the Fermi-level density of states of the Kondo resonance on the quantum dot. Similarly, the Kondo resonance was spectroscopically observed on single magnetic impurities adsorbed on metal surfaces using the STM.[21,22] However in the case of spectroscopic STM experiments, the resonance at the Fermi level appears to have an asymmetric shape and cannot be interpreted simply in terms of the local density of states of the impurity atom. Rather, the electron tunneling current—being a coherent quantum effect—is a result of interference between competing tunneling channels, as will soon be detailed. Unlike in a quantum dot, where the tunneling can take place with appreciable magnitude only through the quantum dot region, the apparent tunneling current from the STM tip to the surface can either go through the resonance localized on the impurity or directly into the conduction states of the surface. The distinction between the conduction and local states will be discussed later. The notion that the tunneling conductance is proportional to the local density of states near the STM tip must then be modified.

In addition to its most common use for observing and determining atomic geometrical structure at surfaces, the STM is used as a sensitive probe of surface electronic structure. Various theoretical approaches to STM conductance employ the tunneling Hamiltonian introduced by Bardeen[23] and golden-rule-type expressions in which under certain limiting conditions of practical interest the STM conductance is indeed determined by the surface density of electronic states near the STM tip.[24,25] Tersoff and Hamann[24] developed a widely used model of the scanning tunneling microscope that includes three dimensionality and the spatial resolution of the tip.

The generic problem of a discrete state interacting with a continuum of states arises in many different areas of physics and chemistry.[26] In condensed-matter physics a frequently occurring realization is the electronic state of an impurity atom immersed within a host lattice.[27,28] In the case of magnetic impurities, the interaction gives rise to nontrivial phenomena such as the Kondo effect.[11–13]

Within the context of atomic physics, Fano discussed related effects, as they might appear on observable absorption line shapes or resonant electron scattering cross sections which are due to the configuration interaction (CI) that couples a discrete two-electron excited atomic state with a continuum of ionization states.[29,30] While the ''natural'' line shape of the resonance is Lorentzian, when studied by experiments in which an external probe interacts with the system, the resonance can appear to have an asymmetric line shape. Such line shapes are referred to as Fano resonances. Fano found that an asymmetry in absorption line shapes is due to interference between the excitation or decay into CI-mixed discrete and continuum states which both couple to the external probe. If the coupling between the probe and continuum is expressed in terms of an energy-independent matrix element t_c, and the interaction between the probe and the localized state (which has already been diluted by admixture into the continuum) by the matrix element $\tilde{t}_a$, then the line shape detected has the form

$$I \propto \frac{[q+2(\omega-\epsilon_0)/\Gamma]^2}{1+[2(\omega-\epsilon_0)/\Gamma]^2}, \tag{1.2}$$

where $q \equiv \tilde{t}_a/(2\pi V t_c)$, with V being the hybridization (or CI) matrix element between the local state and the continuum. The latter coupling results in the discrete state acquiring a width $\Gamma = 2\pi\rho_s V^2$ (ρ_s is the density of continuum states).

In the present paper, we consider the problem of a discrete state embedded in a continuum, using a probe such as the STM that has an atomic scale spatial resolution. This work was motivated by recent STM experiments involving single Kondo impurities.[21,22] The resonance observed in the conductance was interpreted by the authors in terms of the Fano interference. The fit of the resonance to the Fano formula[21]—generalized to the case where intra-atomic Coulomb interaction on the impurity is taken into account—was based on the assumption that tunneling into an Anderson impurity can be extended to include tunneling into the continuum in a straightforward way. Upon further consideration, it appears that this generalization of the Fano result to the case of STM conductance is not as straightforward as was presumed. In the present paper we obtain a more complicated expression than the elementary Fano formula, one which accounts for the correct asymptotic behavior for large tip-impurity separation. In particular, when the dependence of the probe's distance from the local state is properly included, then observable consequences of the local-state admixture with the conduction electrons show the correct asymptotic long-range behavior in the large tip-to-impurity-separation limit, as they obviously should.

The difference between the Fano line shape and the result obtained here is due to the different nature of the probe in the ''multicenter'' STM configuration (one ''center'' on the impurity/discrete state, the other on the STM tip/probe) compared with the ''single-site'' atomic physics processes. While Fano was concerned with light absorption or electron scattering, where the system under study was always at the probe's focus, the outcome of STM experiments must depend upon the variable spatial position of the probe (tip) with respect to the discrete state under investigation. Put another way, for the atomic physics applications considered by Fano, both the discrete state coupled to the continuum and the initially excited decaying or autoionizing state (the ''probe'' state in our STM language) are atomic states spatially localized at the same site by the same atomic central potential. In contrast, the S (scanning) in STM assures that the tip, and hence the initial excited state, can be independently located with respect to the position of the ''discrete state coupled to the continuum,'' and it is this extra degree of freedom that enriches the potential information content in STM line-shape analysis, but also requires a much more detailed theoretical treatment than merely fitting the atomic physics Fano line shape [Eq. (1.2)] to position-dependent STM spectra. This will be expanded upon in depth later. This realization dem-

onstrates the importance and crucial need for considering the measurement process in quantum-mechanical observations.

The structure of the paper is as follows. In Sec. II, we introduce the model of the system, and discuss our approximations. In Sec. III and the supporting appendixes, we develop the general nonequilibrium theory of STM tunneling current and conductance in the presence of an adsorbate-induced resonance. In Sec. IV, we illustrate the predictions and consequences of our theory on two models for the adsorbate: the nonmagnetic and Kondo models.

II. MODEL AND APPROXIMATIONS

Models of scanning tunneling microscopy are abundant in the literature of the last two decades, and standard texts exist.[7–10] We approach the problem as a nonequilibrium process, and discuss the corrections to the Tersoff-Hamann formulation.[24] Our intent is to develop a theory under general and self-consistent assumptions that accurately captures most of the qualitative aspects involved, and do so in a way that make extensions to more realistic calculations formally straightforward. We focus on tunneling through adsorbate resonances. Throughout this paper, we adopt the convention that the energies are measured with respect to the respective Fermi levels of the substrate and tip unless specified otherwise, and set $\hbar=1$. When the tip is biased, we explicitly shift the tip energies.

A. Model of the studied system

We consider a system which consists of a clean metallic surface with a single impurity atom adsorbed on it. The STM will be used to study the system by means of tunneling through a resonance produced by an electronic state of the impurity, such as the $5f$ orbital of Ce/Ag(111) (Ref. 22) or $3d$ orbital in Co/Au(111).[21] Unless otherwise noted, we place the origin of the coordinate system at a point on the surface of the metal directly below the adsorbate. This means that the position of the impurity is $\mathbf{R}_0=(0,0,Z_0)$. The system without the probe is described by the degenerate Anderson Hamiltonian

$$H_s(\mathbf{R}_0)=\sum_a \epsilon_0(\mathbf{R}_0)c_a^\dagger c_a+\sum_{a>a'} U(\mathbf{R}_0)n_a n_{a'}+\sum_{ka} \epsilon_k c_{ka}^\dagger c_{ka} + \sum_{ka} \{V_{ka}(\mathbf{R}_0)c_{ka}^\dagger c_a+\text{H.c.}\}. \tag{2.1}$$

Here ϵ_0 is the energy of the impurity state $\psi_\sigma(\mathbf{r})$, which we assume may be a multiplet of states described collectively by the quantum number $a\equiv(m\sigma)$. In the simplest case, a corresponds to the spin σ, but it may also include the orbital degeneracy (m) in more complicated cases. In this paper, we discuss at most spin-degenerate states with $a=\sigma$ and $N=2$ (degeneracy). By $c_a^\dagger$ we denote the creation operator for this state. ϵ_k is the conduction-band state energy—independent of σ in the absence of magnetic field—with $c_{ka}^\dagger$ being the creation operator for the corresponding Bloch state with symmetry (spin) a common with the impurity state, and V_{ka} is the matrix element for hybridization between the impurity and conduction states. The second term in Eq. (2.1) corresponds to the intra-atomic Coulomb interaction between electrons in the impurity state ψ_a. If the renormalized energy ϵ_0 lies within the conduction band, the bound state broadens into a resonance which in the wide-band limit with which $U=0$, has a Lorentzian shape [Eq. (1.1)].

B. Interaction of the system with the STM tip

When the STM tip is brought near the impurity, electrons can tunnel between the tip and the adsorbate state. This situation is expressed by adding an interaction term to the Hamiltonian:

$$H_{at}(\mathbf{R}_t,\mathbf{R}_0)=\sum_{pa} \{t_{ap}(\mathbf{R}_t,\mathbf{R}_0)c_a^\dagger c_p+\text{H.c.}\}. \tag{2.2}$$

The tip states are denoted by subscript p. The transfer matrix t_{ap} depends on the position of both the adsorbate Z_0 and the tip $\mathbf{R}_t\equiv(\mathbf{R}_\parallel,Z_t)$, referenced to a common origin.

If the STM coupled only to a discrete state with transfer amplitude t_a then the conductance would, in the wide-band limit ($t_{ap}\equiv t_a$, independent of p), be determined by

$$G\propto|t_a|^2\frac{\Gamma}{(\omega-\epsilon_0)^2+(\Gamma/2)^2}, \tag{2.3}$$

and the conductance would thus be directly related to the impurity density of states. This is reminiscent of the defining characteristics from field emission resonance tunneling spectroscopy, in which tunneling from the substrate to vacuum is disproportionately smaller than that from ''good'' adsorbates.[15–17,31] However, since in the STM geometry tunneling directly between the tip and the metal surface can be comparable to (or in excess of) that between the tip and the impurity, the conductance exhibits a more complex behavior than that of a simple impurity local density of states. We take such processes into account through

$$H_{st}(\mathbf{R}_t)=\sum_{pk} \{t_{kp}(\mathbf{R}_t)c_k^\dagger c_p+\text{H.c.}\}, \tag{2.4}$$

where the tunneling matrix element t_{kp} depends on the position of the tip $\mathbf{R}_t$.

C. Model of the STM tip

An important property of the tip is its spatial resolution, as discussed in great detail by many.[6,18,24,32–34] We will consider the tip to be well defined and terminated by a single atom through which the tunneling predominantly takes place. This is the *s*-wave model of Tersoff and Hamann;[24] see Fig. 1. The important features are the following: (a) the tip Hamiltonian is

$$H_t=\sum_p \epsilon_p c_p^\dagger c_p, \tag{2.5}$$

where $c_p^\dagger$ creates an electron in the state $\psi_p(\mathbf{r})$ with energy ϵ_p measured from the Fermi level of the tip ϵ_{Ft}; (b) when the tip is positioned near the surface, tunneling into and out

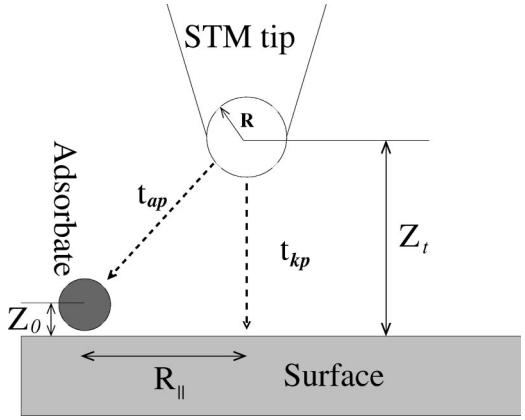

FIG. 1. Schematic picture of the STM.

of a state ψ_p can take place; (c) the states are filled up to the chemical potential ϵ_{Ft} controlled by the bias; (d) the tip states are characterized by a density of states $\rho_t(\omega)$; and (e) the asymptotic form of the tip eigenstate ψ_p in the vacuum region extending toward the metal surface is characterized by the atomic orbital of the apex atom. The wave function ψ_p can be found based on simple physical arguments without solving the complete problem. If ϕ_t is the work function of the tip and $\kappa_t \equiv \sqrt{2m_t^*(\phi_t - \epsilon_p)}$, then, following Tersoff and Hamann,

$$\psi_p(\mathbf{r}) \propto R e^{\kappa_t R} \frac{\exp(-\kappa_t r)}{r}, \tag{2.6}$$

where R is the radius of curvature of the tip about its center, which is located at the origin of this ''tip-defining'' coordinate system. While Eq. (2.6) represents an ''*s*-wave tip,'' more generally ψ_p would carry whatever symmetry was possessed by the relevant atomic orbital centered at the tip apex.[10,18,32] The wave-function tail, controlled by κ, depends on the bias and tip-surface separation. Both factors modify the height of the vacuum barrier, and hence the effective work function ϕ determining κ. These modifications can be essentially included by renormalizing the wave-function tails and the densities of states by position- and energy-dependent factors via the tunneling matrix elements. We discuss the tunneling matrix elements next.

D. Approximations for the tunneling matrix elements

An important role in our formulation is played by the tunneling (hybridization) matrix elements V_{ka}, t_{ap}, and t_{kp} since they include the dependence on electronic structure and the tip and adsorbate position.

We begin with the discussion of the matrix elements V_{ka} and t_{kp} that contain the metal wave functions $\psi_{\mathbf{k}}(\mathbf{r})$. They have the form

$$M_{kl}(\mathbf{R}_l) = \int d^3r\, \psi_{\mathbf{k}}^*(\mathbf{r}) v_{sl}(\mathbf{r};\mathbf{R}) \psi_l(\mathbf{r}-\mathbf{R}_l), \tag{2.7}$$

where v_{sl} is the potential representing the mutual interaction of the two systems. The wave function $\psi_{\mathbf{k}}(\mathbf{r})$ is a Bloch state of the unperturbed metal, and $\psi_l(\mathbf{r}-\mathbf{R}_l)$ is the wave function (in the coordinate system of the metal) of the adsorbate state a in the case of V_{ka} or the tip wave function in the case of t_{kp}. Matrix elements of this type have been the focus of intense study in the context of charge transfer processes at surfaces.[35–40]

The energies ϵ_k of the metal electrons are written in terms of the perpendicular and parallel components as $\epsilon_k \equiv \epsilon_{k_z} + \epsilon_{k_\|}$. We follow the convention that $\epsilon_{k_\|}$ is measured from the bottom of the two-dimensional band and ϵ_{k_z} is measured with respect to ϵ_{Fs}. For example, for the jellium model we write $\epsilon_{kz} = k_z^2/2m_s^* - D$ and $\epsilon_{k_\|} = k_\|^2/2m_s^*$, where $(-D)$ is the energy of the bottom of the band with respect to the Fermi level. The Bloch states can generally be written in the relevant region outside the metal as

$$\psi_{n\mathbf{k}}(\mathbf{r}) = e^{-\kappa_{ns} z} u_{n\mathbf{k}_\|}(\boldsymbol{\rho}, z) e^{i\mathbf{k}_\| \cdot \boldsymbol{\rho}}, \tag{2.8}$$

where n is the band index, $u_{n\mathbf{k}_\|}(\boldsymbol{\rho},z)$ is a function weakly dependent on z outside the surface and periodic in $\boldsymbol{\rho}$, the electron coordinate in the plane of the surface. This form is equally valid for the metal band-gap surface states that have come to seem ubiquitous to STM studies on (111) noble metal surfaces.

For jellium, $u_{n\mathbf{k}_\|}(\mathbf{r})$ is constant, and the metal states are then simply plane waves along the surface with exponentially decaying amplitude into the vacuum. Here $\kappa_{ns} = \sqrt{2m_s^*(\phi_s - \epsilon_{nk_z})} = \sqrt{2m_s^*(\phi_s - \epsilon_{nk} + \epsilon_{nk_\|})}$, with m^* the metal electron effective mass (number) and ϕ_s the height of the tunneling barrier for a Fermi-level electron. For bias voltages much smaller than the work function, ϕ_s is equal to the metal work function. We omit the band index n in the rest of the paper. We also define $\lambda_\omega^{-1} = \sqrt{2m_s^*(\phi_s - \omega)}$, where the energy factor $(\phi_s - \omega)$ represents the effective tunneling potential barrier for an electron with energy ω. For small bias voltages, $\omega \approx 0$, and we can replace λ_ω, which depends weakly on energy in this range, by its Fermi level value $(\equiv\lambda)$.

The integrand of the matrix elements [Eq. (2.7)] is well localized outside the surface where the Bloch states are of the form of Eq. (2.8). We can shift its arguments and approximate the matrix elements by $M_{kl}(\mathbf{R}_l) \simeq M_0 \psi_{\mathbf{k}}^*(\mathbf{R}_l)$, where M_0 is the overlap integral, defined in Eq. (2.7), that contains the dependence of the matrix element on the symmetry of the atomic orbitals near the tip. We then write V_{ka} as

$$V_{ka}(\mathbf{R}_0) \simeq V_a(Z_0) \psi_{\mathbf{k}}^*(0), \tag{2.9}$$

where $V_a(Z_0) = V_0 e^{-Z_0/\lambda}$. In the case of the tip-to-surface tunneling matrix element t_{kp} it is convenient to isolate the k-independent part of its z dependence defined as $t_c(Z_t) = t_0 e^{-Z_t/\lambda}$, and write the matrix element in the form

$$t_{kp}(\mathbf{R}_t) = t_c(Z_t) e^{Z_t/\lambda} \psi_{\mathbf{k}}^*(\mathbf{R}_t). \tag{2.10}$$

We note that the *s*-wave tip-to-surface tunneling matrix element t_{kp} was shown by Tersoff and Hamann[24] under quite general assumptions to assume the form of Eq. (2.10) with

the tip wave function given by Eq. (2.6), which indicates that our simple qualitative arguments are supported by a more detailed analysis.

The tip-to-impurity matrix element

$$t_{ap}(\mathbf{R}_t,\mathbf{R}_0)=\int d^3r\ \psi^*_{\mathbf{p}}(\mathbf{r}-\mathbf{R}_t)v_{at}(\mathbf{r};\mathbf{R}_t,\mathbf{R}_0)\psi_a(\mathbf{r}-\mathbf{R}_0) \tag{2.11}$$

depends on the position of both the adsorbate (Z_0) and the tip ($\mathbf{R}_t$). Since tunneling from the tip takes place predominantly through the apex atom, the matrix element t_{ap} will reflect the symmetry and spatial dependence of the states localized on the adsorbate and in the tip apex. With ψ_p and ψ_a appearing in Eq. (2.11), both atomiclike functions in the relevant region of overlap centered respectively on the tip and on the adatom, in a broad sense t_{ap} is similar to a common two-center hybridization/hopping integral defining the binding in a diatomic molecule.[41,42] Based on this analogy from quantum chemistry, t_{ap} given by Eq. (2.11) should take the form

$$t_{ap}(\mathbf{R}_t,Z_0)\approx t_a e^{-|\mathbf{R}_t-Z_0\hat{i}_z|/\alpha}\equiv t_a(\mathbf{R}_t,Z_0). \tag{2.12}$$

Here $\alpha^{-1}\approx[\kappa_t+\sqrt{2m(\phi_s-\epsilon_0)}]$ is an effective decay constant evaluated for states at the Fermi level of the tip; $|\mathbf{R}_t-Z_0\hat{i}_z|=\sqrt{R_\parallel^2+(Z_t-Z_0)^2}$ is the tip-to-atom separation, as depicted in Fig. 1, where $\mathbf{R}_\parallel$ is the parallel component of $\mathbf{R}_t$. The decay constant κ_t depends on the energy of the tip state (ϵ_p), but this dependence is very weak for small biases considered here and we neglect it. In this case, the matrix element is well approximated by the p-independent form $t_a(\mathbf{R}_t,Z_0)$. The matrix element t_a may be taken as real.

III. NONEQUILIBRIUM THEORY OF THE TUNNELING CURRENT AND DIFFERENTIAL CONDUCTANCE

The tunneling between the adsorbate-metal complex and a biased tip is a nonequilibrium process. Although in this paper we frequently make the assumption that the tip-system interaction is weak enough so that local equilibrium is maintained to a good approximation, the assumption is less valid when the tip is near the surface. For this reason, we develop our theory of the tunneling process within the Keldysh-Kadanoff[43,44] framework for the nonequilibrium Green's functions, and discuss the nonequilibrium corrections.

A. General expression for the tunneling current in terms of nonequilibrium Green's functions

We define the tunneling current as the flow of electrons through a closed surface around the tip. It is expressed in terms of the continuity equation as

$$I=-e\left\langle\frac{dn_t(t)}{dt}\right\rangle, \tag{3.1}$$

where $n_t=\Sigma_p c_p^\dagger c_p$ is the number operator for the tip electrons, and the brackets signify the ensemble average, which in the local equilibrium case is the thermal average over the tip states. The time derivative is found from the Schrödinger equation of the total Hamiltonian of the tip-substrate-adsorbate system $H_{\rm tot}=H_s+H_t+H_{at}+H_{st}$. Since the number operator commutes with H_s and H_t, the only contribution comes from the interaction terms H_{at} and H_{st}, and the current is

$$I=\frac{2e}{\hbar}\mathrm{Im}\left\{\sum_{kp}\ t_{kp}\langle c_k^\dagger(t)c_p(t)\rangle+\sum_{ap}\ t_{ap}\langle c_a^\dagger(t)c_p(t)\rangle\right\}, \tag{3.2}$$

where we omitted the arguments in t_{kp} and t_{ap} for convenience, and used the relation $t_{ap}=t_{pa}^*$ and $t_{kp}=t_{pk}^*$. We write the arguments explicitly only when we wish to emphasize their dependence. We define the time loop Green's functions $G_{pa}(t,t')=-i\langle T_C c_p(t)c_a^\dagger(t')\rangle$ and $G_{pk}(t,t')=-i\langle T_C c_p(t)c_k^\dagger(t')\rangle$, where T_C orders the times along a contour C in the complex time plane. The contour can be taken to be the Kadanoff-Baym contour,[44] the Keldysh contour,[43] or a more general choice. The discussion of nonequilibrium Green's function is available in standard books and review articles,[44–46] and we refer the reader to these references for further details. Our notation follows closely that of the more detailed discussion in Ref. 47. In the present paper, we are mainly interested in the steady-state tunneling current (time independent), and therefore we work with the Fourier transformed quantities in frequency rather than time space. The current can be written as

$$I=\frac{2e}{h}\mathrm{Im}\int_{-\infty}^{\infty}d\omega\left\{\sum_{kp}\ t_{kp}G_{pk}^<(\omega)+\sum_{ap}\ t_{ap}G_{pa}^<(\omega)\right\}, \tag{3.3}$$

where $G_{pk}^<(\omega)$ and $G_{pa}^<(\omega)$ are the Fourier transforms of $G_{pk}^<(t,t')=\langle c_k^\dagger(t')c_p(t)\rangle$ and $G_{pa}^<(t,t')=\langle c_a^\dagger(t')c_p(t)\rangle$—the analytic pieces on the real-time axis of the Green's functions introduced above. Equivalently, the current may be calculated from $\langle(dn_s/dt)+(dn_a/dt)\rangle$. It is easy to see that this approach also leads to Eq. (3.2).

The problem of finding the current thus reduces to finding the ''lesser'' Green's functions $G_{pa}^<$ and $G_{pk}^<$. This is done using the equation of motion method for the time-ordered Green's functions in Appendix B.

We substitute solution (B4) and (B9) for G_{pa} and G_{pk} from Appendix A into Eq. (3.3), and write the tunneling current in the form

$$I=\frac{2e}{h}\mathrm{Im}\int_{-\infty}^{\infty}d\omega\sum_{pp'}\{G_{pp'}^R(\omega)T_{p'p}^<(\omega)+G_{pp'}^<(\omega)T_{p'p}^A(\omega)\}, \tag{3.4}$$

where the $T_{pp'}(\mathbf{R}_t,\mathbf{R}_0,\omega)$ matrix for scattering of the tip electrons from the adsorbate-metal complex is defined by

$$T_{pp'}=\sum_k\ t_{pk}G_k^0t_{kp'}+\sum_a\ \tilde{t}_{pa}G_a\left(t_{ap'}+\sum_k\ \tilde{V}_{ak}G_k^0t_{kp'}\right), \tag{3.5}$$

with

$$\tilde{V}_{ka} = V_{ka} + \sum_p t_{kp} G_p^0 t_{pa} \tag{3.6}$$

and

$$\tilde{t}_{pa} = t_{pa} + \sum_k t_{pk} G_k^0 V_{ka}, \tag{3.7}$$

the hybridization and tunneling matrix elements for the adsorbate modified by the tip-substrate interaction. The matrix $T_{pp'}$ incorporates the properties of the tip as well as the adsorbate into the expression for current. We discuss its physical meaning more in Sec. III B.

B. Tunneling current at large tip-surface separation

We define the equilibrium tunneling current as the large tip-surface separation limit of Eq. (3.4) when the tip and the adsorbate-substrate complex are each in local equilibrium. This is equivalent to keeping only the lowest-order terms in t_{kp} and t_{pa}. In our formalism, this is achieved by replacing $\tilde{G}_{pp'} \to G_p^0 \delta_{pp'}$ in Eq. (3.4) and $\tilde{V}_{ka} \to V_{ka}$ in $T_{pp'}$, and by using the fluctuation-dissipation relation $G_i^<(\omega) = f_i(\omega)\rho_i(\omega)$. The subscript i stands for the tip (t), adsorbate (a), and metal (s), respectively. The adsorbate is in equilibrium with the metal, i.e., $f_a(\omega) = f_s(\omega)$. The matrix $T_{pp'}$ is expressed entirely in terms of the Green's functions of the system and the tunneling matrix elements t_{pk} and t_{pa}. Since these matrix elements reflect the symmetry of the apex atom wave function, but are only weakly dependent on p on the energy scale of the resonance width, the matrix $T_{pp'}$ will also have this property. We therefore make an additional assumption that $\Sigma_p G_p^0 T_{pp} \sim (\Sigma_p G_p^0) T_t$, where

$$T_t = \sum_k t_{pk} G_k^0 t_{kp} + \sum_a \tilde{t}_{pa} G_a \tilde{t}_{ap} \tag{3.8}$$

is only a function of the atomic tip orbital independent of p. We define a tip-specific quantity observable by the STM, which is related to the local density of states

$$\tilde{\rho}_{\rm sat}(\mathbf{R}_t, \mathbf{R}_0; \omega) = -\frac{1}{\pi} \mathrm{Im}\, T_t^R(\mathbf{R}_t, \mathbf{R}_0; \omega), \tag{3.9}$$

and write the equilibrium current $I_{\rm eq}(\mathbf{R}_t, \mathbf{R}_0, V)$ as

$$I_{\rm eq} = \frac{2e}{h} \int_{-\infty}^{\infty} d\omega [f_t(\omega') - f_s(\omega)] \rho_t(\omega') \tilde{\rho}_{\rm sat}(\omega), \tag{3.10}$$

where ρ_t is the density of tip states and $\omega' = \omega - eV$, with V being the bias voltage. This equation is easily related to traditional formulations given in terms of an integral product of an electron ''supply function'' multiplied by a tunneling or transmission probability[1–3,15,17] when it is realized that $\tilde{\rho}_{\rm sat}$, as defined here, already contains within it factors $(\propto |t|^2)$ representing the role of the tunneling probability.

This expression has a form similar to the standard tunneling theories which express the current as a product of the local densities of states of the two systems evaluated at a common point and a difference in the corresponding Fermi functions. Kawasaka and co-workers,[48,49] who studied the STM current through a Kondo resonance, used as a starting point of their considerations the Tersoff-Hamann expression[24]

$$I_{eq} \propto \int d\omega [f_t(\omega') - f_s(\omega)] \rho_t(\omega') \rho_{sa}(\mathbf{R}_t, \omega) \tag{3.11}$$

according to which the current at zero temperature is related to the local density of states (LDOS) of the adsorbate plus metal electrons $\rho_{sa}(\mathbf{R}_t, \omega)$ at the position of the tip, where the local density of states is

$$\rho_{sa}(\mathbf{R}_t, \omega) = -\frac{1}{\pi} \mathrm{Im} \langle \mathbf{R}_t | G^R(\omega) | \mathbf{R}_t \rangle. \tag{3.12}$$

The LDOS is expressed in terms of unperturbed metal and adsorbate states by inserting $\Sigma_k |k\rangle\langle k| + |a\rangle\langle a| (\approx 1)$ on both sides of G in Eq. (3.12). This is strictly valid only for orthogonal orbitals, $\langle a|k\rangle = 0$. The four resulting terms, proportional to G_a, G_{ka}, G_{ak}, and $G_{kk'}$, reflect the fact that the LDOS includes both adsorbate and metal states perturbed by their mutual interaction. Inserting this expansion into Eq. (3.12) gives, for $\rho_{sa}(\mathbf{R}_t, \omega)$,

$$\rho_{sa} = -\frac{1}{\pi} \mathrm{Im} \Bigg\{ \sum_a |\psi_a|^2 G_a^R + \sum_{ka} \psi_{\mathbf{k}} G_{ka}^R \psi_a'^* + \sum_{ka} \psi_a G_{ak}^R \psi_{\mathbf{k}}^* + \sum_{kk'} \psi_{\mathbf{k}'} G_{k'k}^R \psi_{\mathbf{k}}^* \Bigg\}, \tag{3.13}$$

where the wave functions are evaluated at $\mathbf{R}_t$.

Comparison of Eqs. (3.13) and (3.11) and (3.8) and (3.10) shows the difference between our equilibrium limit and the transfer Hamiltonian method.[2,23] The tunneling current and differential conductance in the equilibrium limit provides information about $\tilde{\rho}_{\rm sat}$—a local density of states modified by the tunneling matrix elements—rather than the LDOS. In the case when the tunneling takes place into distinct orbitals with different symmetry, $\tilde{\rho}_{\rm sat}$ can be rather different from ρ_{sa} and the statement that the STM is a measure of local density of states must be understood in this context.

We now evaluate $\tilde{\rho}_{\rm sat}$ in Eq. (3.10), and write the equilibrium current using approximations (2.9), (2.10), and (2.12) for the tunneling matrix elements. We note that the approximations do not require any specification of the substrate electronic structure. The final form of the current allows a discussion of the tunneling resonances in terms of the well-established Fano line shapes.

We introduce quantities in terms of which the current is expressed. First, we define the ''bulk'' density of states for the substrate and the tip as $\rho_s(\omega) = \Sigma_k \delta(\omega - \epsilon_k)$ and $\rho_t(\omega) = \Sigma_p \delta(\omega - \epsilon_p)$. The impurity width without the STM tip is defined as

$$\Gamma_{as} \langle \mathbf{R}_0, \omega \rangle = 2\pi \rho_s(\omega) V_a^2(\mathbf{R}_0). \tag{3.14}$$

The adsorbate perturbation on the local density of conduction states at some lateral position between the tip and the adsorbate is discussed in terms of the unperturbed substrate Green's function

$$G_0^+(\mathbf{r},\mathbf{r}';\omega)=\sum_k \frac{\psi_k(\mathbf{r})\psi_k^*(\mathbf{r}')}{\omega-\epsilon_k+i\eta}. \tag{3.15}$$

We define two dimensionless quantities related to the real and imaginary parts of the Green's function

$$\Lambda(\mathbf{R},\omega)=e^{Z/\lambda}\frac{\mathrm{Re}\,G_0^+(\mathbf{R},0;\omega)}{\pi\rho_s(\omega)} \tag{3.16}$$

and

$$\gamma(\mathbf{R},\omega)=-e^{Z/\lambda}\frac{\mathrm{Im}\,G_0^+(\mathbf{R},0;\omega)}{\pi\rho_s(\omega)}. \tag{3.17}$$

These two functions carry the information about both the spatial extent of the metal electron perturbation at arbitrary $\mathbf{R}$ in the surface region due to a localized perturbation at $\mathbf{R}_\parallel=0$, and also the spatial resolution of the tip, as we will see later. We have included the exponential factor $e^{Z/\lambda}$ in definitions (3.16), (3.17), and (3.18) because we explicitly take the k-independent part of the exponential dependence on position to be part of the tunneling matrix elements $V_a(Z_0)$, $t_a(\mathbf{R}_t,Z_0)$, and $t_c(Z_t)$. We postpone further discussion of $G_0^+(\mathbf{r},\mathbf{r}',\omega)$ to Sec. III E.

Finally, we define a dimensionless quantity as the normalized density of the substrate states at a position $\mathbf{R}$ above the metal surface:

$$\nu(\mathbf{R},\omega)=e^{2Z/\lambda}\frac{\rho_s(\mathbf{R},\omega)}{\rho_s(\omega)}=-e^{2Z/\lambda}\frac{\mathrm{Im}\,G_0^+(\mathbf{R},\mathbf{R};\omega)}{\pi\rho_s(\omega)}. \tag{3.18}$$

The tunneling current I_0 into a clean metal is given by the first term in Eq. (3.8). The current I_0 for small bias ($V/\phi_s \ll 1$) can be written with the above definitions in a familiar form

$$I_0(\mathbf{R}_t,V)=\frac{2e}{h}\int_{-\infty}^{\infty}d\omega\,\rho_t(\omega')\times[f_t(\omega')-f_s(\omega)]\rho_s(\omega)\pi t_c^2(\mathbf{R}_t)\nu(\mathbf{R}_t;\omega). \tag{3.19}$$

Here, $f_s(\omega)$ and $f_t(\omega)$ are the substrate and STM tip Fermi functions, respectively, and $\omega'=\omega-eV$. The tip and substrate are assumed to have common chemical potential $\epsilon_{Fs}=\epsilon_{Ft}=0$ at zero bias $eV=0$, and we adopt the convention of measuring the energies in the substrate-adsorbate complex and in the tip from their respective Fermi levels at finite bias. The bias V is measured with respect to ϵ_{Fs} and is defined as positive when the chemical potential of the tip ϵ_{Ft} is raised. The functions ρ_s and ρ_t are the substrate and tip densities of states, respectively.

The equilibrium current in the presence of the adsorbate is written by expressing $\tilde{\rho}_{\mathrm{sat}}$ with the notation and approximations that lead to Eq. (3.19). We define a modified matrix element $\tilde{t}_a(\mathbf{R}_t,\mathbf{R}_0;\omega)$ for tunneling from the tip to the adsorbate state as

$$\tilde{t}_a=t_a+\pi t_c\rho_s\Lambda V_a. \tag{3.20}$$

The second term represents a coherent process of tip-to-surface tunneling, through-surface propagation, and surface-to-adsorbate hopping. This is completely isomorphic with Fano's coupling of an excited state (here the tip state), with the originally discrete state ''modified by admixture of states of the continuum.'' The reader is enthusiastically directed to Fano's original paper for further enlightenment on this point.

We introduce the Fano[29] parameter $q(\mathbf{R}_t,\mathbf{R}_0;\omega)$ as

$$q=\frac{\tilde{t}_a}{\pi t_c V_a\rho_s}. \tag{3.21}$$

We will see later that this definition of q makes the expression for differential conductance formally equivalent to the Fano formula in certain limits. It is now rather straightforward to evaluate $\tilde{\rho}_{\mathrm{sat}}$ using Eqs. (3.8) and (3.9) in Eq. (3.10). After rearranging the terms, we write the current $I_{\mathrm{eq}}(\mathbf{R}_t,\mathbf{R}_0,\omega)$ in the presence of the adsorbate resonance as

$$I_{\mathrm{eq}}(\mathbf{R}_t,\mathbf{R}_0,V)=\frac{2e}{h}\int_{-\infty}^{\infty}d\omega\,\rho_t(\omega')\times[f_t(\omega')-f_s(\omega)]\rho_s(\omega)\pi t_c^2(\mathbf{r}_t)\times Y(\mathbf{R}_t,\mathbf{R}_0,\omega), \tag{3.22}$$

with

$$Y=\nu+\sum_a\frac{\Gamma_{as}}{2}\{(\gamma^2-q^2)\mathrm{Im}\,G_a^R+2q\gamma\,\mathrm{Re}\,G_a^R\}. \tag{3.23}$$

In our approximation, the localized nature of the tip and the adsorbate enters through the position dependence of $t_a(\mathbf{R}_t,Z_0)$ and the substrate Green's function $G_0^+(\mathbf{R}_t,0;\omega)$. The matrix element t_a gives an exponentially decreasing amplitude with increasing tip-adsorbate distance, and the substrate Green's function gives decreasing amplitude due to the phase difference between electrons entering (or leaving) the surface at the adsorbate site and leaving (or entering) at $(\mathbf{R}_\parallel, z=0)$, and also due to the exponential decay of the tip wave function with increasing $k_\parallel$. We note that, in the wide-band limit for the substrate and with the tip near the surface above the adsorbate, $\tilde{t}_a\approx t_a$, since in this limit $\mathrm{Re}\,G^+$ and thus Λ vanish.

Finally it follows from Eq. (3.22) that the tunneling current I_{eq} is independent of temperature if ρ_t, ρ_s, and $Y(\mathbf{R}_0,\mathbf{R}_t,\omega)$ are independent of energy in the relevant energy range. If ρ_s shows a structure on the scale of the temperature T while ρ_t is constant, the current will depend on the temperature of the tip only. The same is true for $\mathcal{G}$, the differential conductance.

C. Differential conductance in the limit of large tip-surface separation

The differential conductance is obtained directly from Eq. (3.22) by differentiating it with respect to the bias, i.e., $\mathcal{G} = dI/dV$. We do this here under the assumption that the bias voltage is varied across a sufficiently narrow range so that the density of tip states may be taken to be constant. Under these assumptions the differential conductance $\mathcal{G}_{\rm eq}$ is

$$\mathcal{G}_{\rm eq}(\mathbf{R}_t,\mathbf{R}_0,V)=\frac{2e^2}{h}\int_{-\infty}^{\infty}d\omega\,\rho_t(\omega')\times\left(-\frac{\partial f_t(\omega')}{\partial\omega}\right)\rho_s(\omega)\pi t_c^2(\mathbf{R}_t)Y(\mathbf{R}_t,\mathbf{R}_0;\omega), \tag{3.24}$$

and, for the clean metal,

$$\mathcal{G}_0(\mathbf{R}_t,V)=\frac{2e^2}{h}\int_{-\infty}^{\infty}d\omega\,\rho_t(\omega')\times\left(-\frac{\partial f_t(\omega')}{\partial\omega}\right)\rho_s(\omega)\pi t_c^2(\mathbf{R}_t)\nu(\mathbf{R}_t,\omega). \tag{3.25}$$

These expressions neglect any changes to the tunneling barrier from the finite bias voltage. When these approximations are not justified, the conductance must be obtained by differentiating the expressions for the current [Eqs. (3.22) and (3.19)]. This is always the case for $I_{\rm tot}$ of Sec. III B when nonequilibrium effects are important.

D. Nonequilibrium effects at stronger tip-surface coupling

We now generalize Eq. (3.22) for the equilibrium tunneling current—obtained in the lowest order in t_{ap} and t_{kp}—by including nonequilibrium effects. The general problem of tunneling for arbitrary relative strength between the tunneling amplitudes t_{ap} and t_{kp} and the hybridization matrix V_{ak} and for finite bias is formulated in Eq. (3.4), but the expression is quite complicated to evaluate in practice. In a typical STM experiment, the tunneling matrix elements t_{ap} and t_{kp} are much smaller than V_{ak}. We can expect the nonequilibrium effects to be important when, at small separations, the magnitude of the two tunneling matrix elements is not a negligible fraction of $|V_{ak}|$. However, we can always safely assume that $|t_{ak}|$ and $|t_{ap}|$ are smaller than $|V_{ak}|$ in the STM experiments under all realistic conditions.

Therefore we make additional simplifications which are justified by these relations. First of all, we replace $\tilde{V}_{ak}$ by V_{ak} inside Eqs. (3.5) and (A5). We neglect the modifications to the tip and substrate wave functions, i.e., replace $\tilde{G}_{kk'}$ by $\delta_{kk'}G_k^0$ and $\tilde{G}_{pp'}$ by $\delta_{pp'}G_p^0$. We also neglect any deviations from thermal electronic distribution in the substrate and tip, i.e., we assume the validity of the fluctuation-dissipation theorem for the tip and substrate Green's functions. On the other hand, when the tip-adsorbate coupling is not negligible with respect to the adsorbate-metal hybridization, the current into the resonance can be large enough to produce a significant nonequilibrium electronic population on the adsorbate, since the time scales for electron dissipation from the resonance into the metal and tip, respectively, are comparable. In this case, the fluctuation-dissipation theorem $G_a^<=f_s\rho_a$ is no longer valid for the adsorbate Green's function, and we must use the full nonequilibrium $G_a^<(\omega)$ instead of $f_s(\omega)\rho_a(\omega)$ in Eq. (3.22).

Under these assumptions, we find it convenient to write the total current with the nonequilibrium effects as $I_{\rm tot}=I_{\rm eq}+\delta I_{\rm non}$, where $I_{\rm eq}$ is formally given by Eq. (3.22) and $\delta I_{\rm non}$ is

$$\delta I_{\rm non}=-\frac{2e}{h}\sum_a\int_{-\infty}^{\infty}d\omega\,\pi^2\rho_t\rho_s^2t_c^2V_0^2\times(f_s\,{\rm Im}\,G_a^R+\pi G_a^<)(q^2+\gamma^2), \tag{3.26}$$

where all adsorbate and substrate densities and Green's functions are evaluated at energy ω and ρ_t at $\omega'=\omega-eV$. We omitted the spatial arguments for simplicity. The bias dependence enters through the self-consistent solution of the adsorbate spectral density $\rho_a(\omega)=-(1/\pi){\rm Im}\,G_a^R(\omega)$ and the ''lesser'' Green's function $G_a^<(\omega)$. In the case of a noninteracting system ($U=0$), the spectral density does not depend on the bias and the only nonequilibrium (finite bias) effect is given by the difference between the equilibrium $G_{a,{\rm eq}}^<(\omega)=f_s(\omega)\rho_a(\omega)$ and the nonequilibrium density of occupied states $G_a^<(\omega)$, as featured in $\delta I_{\rm non}$.

On the other hand, the spectral density $\rho_a(\omega)$ of Kondo systems itself depends on the bias. This means that $I_{\rm eq}$ also contains nonequilibrium effects, and is different from the equilibrium current despite the subscript ''eq'' and its identical form. The effect of bias on the spectral function depends on the tip hybridization with the discrete impurity level, and is similar to that of temperature for $eV\leqslant T_K$ where it broadens the Kondo resonance. At larger biases the broadening increases further, and a second peak may develop at the Fermi level of the tip, depending on the strength of the adsorbate-to-tip hybridization $\Gamma_{at}=2\pi\rho_t t_a^2$ compared to $\Gamma_{as}=2\pi\rho_s V_a^2$ for the relevant impurity orbital.[50,51] In Fig. 2, for different bias voltages we show the spectral function and electron occupation of the resonance for a model Kondo system with Γ_{at} equal to $\sim$10% of Γ_{as} and under an additional assumption that $|t_{kp}|\ll|t_{ap}|$. The model will be discussed in more detail in Sec. IV B.

E. Substrate Green's function G_0^+ and perturbation of the conduction electrons: jellium surface

There are two ways in which the adsorbate state affects the tunneling conductance: (a) direct tunneling into the discrete state; and (B) perturbation of the conduction electron states by the discrete state, which consequently contributes to the tip-to-continuum tunneling current. Therefore, the presence of an impurity on the surface can be sensed spectroscopically even if the direct tunneling into the resonance is negligible as is the case, for instance, of Ce/Ag(111).[22] Both contributions drop off with increasing tip-adsorbate separa-

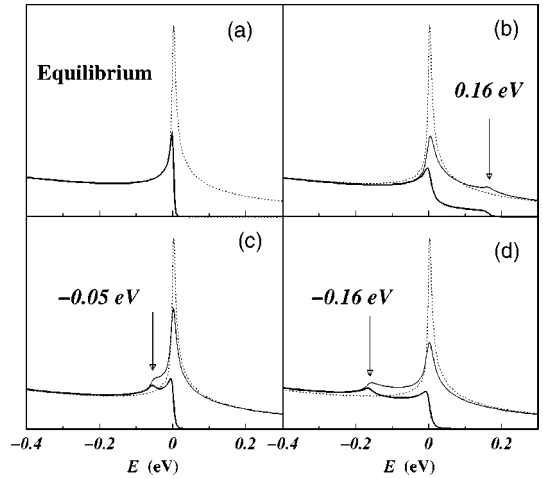

FIG. 2. The spectral function $\rho_a(\omega)$ and the occupied density of states of a model Kondo system as a function of bias voltage at small metal-tip separation given by $\Gamma_{at}=0.1\Gamma_{as}$. (a) Equilibrium, (b)–(d) finite bias. Bold line, electron population; solid thin, spectral density; dotted line, equilibrium spectral density.

tion. The direct tunneling into the resonance is controlled by $t_{ap}(\mathbf{R}_t,Z_0)$, which is a function of the overlap between the tip and adsorbate wave function, and thus decays exponentially with the distance. The perturbation of the continuum also vanishes at large distances from the adsorbate. However, its spatial extent shows a more complicated behavior, and depends on the details of the electronic structure of the substrate in resonance with the broadened discrete state. Its position dependence enters through the Green's function $G_0^+(\mathbf{R}_t,0;\omega)$. We note that the imaginary part γ appears explicitly in the expression for the conductance [Eq. (3.24)], while the real part Λ enters the definition of $\tilde{t}_a$.

We consider a simple approximation for G_0^+ based on the assumption that in the relevant surface region the surface corrugations are smoothed out (jellium model) and both the Bloch and/or surface state ψ_k [Eq. (2.8)] are given by

$$\psi_{\mathbf{k}}(\mathbf{r})\propto e^{-\kappa_s z}e^{i\mathbf{k}_\parallel\cdot\boldsymbol{\rho}}. \tag{3.27}$$

The states with the smallest κ_s have the longest tail into the vacuum region, and thus will be the most important ones in the tunneling process. These are the states with the smallest $\epsilon_{k_\parallel}$. It is then reasonable to represent κ_s in terms of the Taylor expansion around the minimum of $\epsilon_{k_\parallel}$, with ϵ_k equal to the bias. In most cases, it is reasonable to replace ϵ_k by its Fermi-level value. We expand $\epsilon_{k_\parallel}$ around its minimum as $\epsilon_{k_\parallel}\approx k_\parallel^2/2m^*$, and write $\kappa_s=\lambda^{-1}+\lambda k_\parallel^2/2$ plus higher-order terms which we neglect. We then write

$$\psi_{\mathbf{k}}(\mathbf{r})\approx e^{-z/\lambda}e^{-\lambda z k_\parallel^2/2}e^{i\mathbf{k}_\parallel\cdot\boldsymbol{\rho}}. \tag{3.28}$$

As we will show later, the second exponential $e^{-\lambda Z_t k_\parallel^2/2}$ is a measure of the tunneling current carrying $k_\parallel$, the property that gives the STM tip its spatial resolution, and the third exponential $e^{i\mathbf{k}_\parallel\cdot\mathbf{R}_\parallel}$ controls the dependence of the tunneling current on the lateral tip position.

With this approximation for Bloch states in the surface region the substrate Green's function [Eq. (3.15)] is

$$G_0^+(\mathbf{R}_t,0;\omega)=e^{-Z_t/\lambda}\sum_k \frac{e^{-\lambda Z_t k_\parallel^2/2}e^{i\mathbf{k}_\parallel\cdot\mathbf{R}_\parallel}|\psi_k(0)|^2}{\omega-\epsilon_k+i\eta}. \tag{3.29}$$

For the bulk band state propagation, it is easy to show, using Eq. (3.17), that

$$\gamma(\mathbf{R}_t,\omega)=\int_0^1 dx\, J_0(k_\omega R_\parallel\sqrt{1-x^2})e^{-\lambda Z_t k_\omega^2(1-x^2)/2} \tag{3.30}$$

and

$$\Lambda(\mathbf{R}_t,\omega)=\frac{1}{\pi\rho_s(\omega)}\mathcal{P}\int_0^{2D} d\epsilon\,\rho_s(\epsilon)\frac{\gamma(\mathbf{R}_t,\epsilon)}{\omega-\epsilon}, \tag{3.31}$$

where J_0 is the zeroth-order Bessel function and k_ω is the wave vector of the substrate state of energy ω. The normalized density of (STM-accessible) conduction states $\nu(Z_t)$ a distance Z_t from the surface is

$$\nu(Z_t,\omega)=\int_0^1 dx\, e^{-\lambda Z_t k_\omega^2(1-x^2)}. \tag{3.32}$$

In calculating Λ, γ, and ν, we assumed a jelliumlike dispersion relation $\omega=k_\omega^2/2m^*$, and used a parabolic density of states $\rho_s(\omega)=1-\omega^2/D^2$. The incompatibility of the density of states with the dispersion relation is not important for the purpose of demonstrating the important band-structure effects at this level of simplification.

Although expressions (3.30)–(3.32) are valid for a very simple model of the surface, we believe they contain the most important features of more realistic bulk electronic structures. At large Z_t, the dominant contribution to the integral in γ comes from small values of the argument y in $J_0(y)$. In this case, we use the mean value theorem to write Eq. (3.30) as $\gamma(\mathbf{R}_t,\omega)=J_0(\bar{k}R_\parallel)e^{-\lambda Z_t\bar{k}^2/2}$, where $\bar{k}=\alpha k_\omega$ with $\alpha\in(0,1)$. Clearly, $\alpha\to 0$ as $Z_t\to\infty$ and $\gamma(\mathbf{R}_t,\omega)$ is independent of the lateral tip position. Since at the same time $\Lambda\to 0$ and $t_a\to 0$, the STM has no spatial resolution in this limit. As the tip moves closer to the surface the spatial resolution increases. In the limit $Z_t=0$, the integral in Eq. (3.30) can be evaluated, and $\gamma(\mathbf{R}_t,\omega)=j_0(k_\omega R_\parallel)$, where j_0 is the spherical Bessel function of zeroth order.

As our estimates for $t_a(R_\parallel)$ and $\gamma(R_t)$ indicate, the direct tunneling matrix element $t_a(R_\parallel)$ falls off much more rapidly with $R_\parallel$ than does γ. This is due to the limited spatial extent of the tightly bound impurity orbital. Therefore, the relative importance of tunneling into the perturbed continuum is likely to increase with the tip-adsorbate separation. Using a simple model for G^+, we show the typical length scales in Fig. 3(a). We plot t_a (bold solid line) parametrized as $t_a\propto e^{-R_\parallel/\alpha}$ and normalized to one for $R_\parallel=0$ together with γ evaluated at three different positions Z_t above the surface and with $k_\omega=1.2\,\text{Å}^{-1}$. The exponential fall-off for conduction states at the Fermi level with work functions in the range

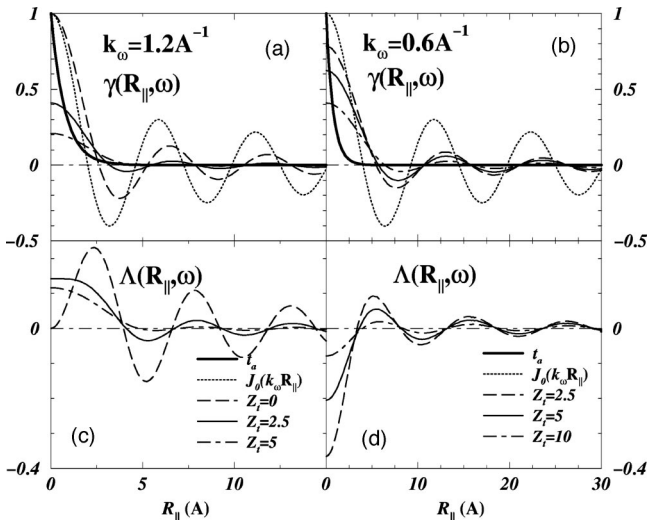

FIG. 3. (a) and (b) show the typical spatial dependence of the tunneling matrix element t_a (bold) and of the substrate Green's function G^+ for the jellium model evaluated at $k_\omega = 1.2\,\text{Å}^{-1}$ (left panels) and $k_\omega = 0.6\,\text{Å}^{-1}$ (right panels) for different Z_t. We parametrize $t_a \propto e^{-R_\parallel}/a$, with $a = 0.75$ Å. Also shown is the Bessel function $J_0(k_\omega R_\parallel)$ for the same k_ω, i.e., γ of a surface state with k_ω. The lower panels (c) and (d) show Λ, and the upper panels (a) and (b) show γ, J_0, and t_a. The comparison for the two wave vectors assumes identical barriers (damping constant λ).

4–5 eV can be characterized by $\lambda = 0.9$ Å. The tightly bound discrete state will have a larger decay constant and we parametrize it by $\alpha = 0.75$ Å. Clearly, γ decays much slower than t_a at small tip-surface separations, but the difference in fall-off becomes smaller with increasing Z_t. We also see by comparison with the Bessel function $J_0(k_F R_\parallel)$ (light dotted line) that the spatial frequency decreases with increasing Z_t and the oscillations eventually disappear entirely. This is due to the fact that smaller k-vectors have larger weight in the tunneling at greater Z_t [see integral (3.30)]. The real part Λ, shown in Fig. 3(c) for the same k vector, has a similar behavior. However, being a Hilbert transform of the imaginary part, the nodes in Λ appear at the positions of local extrema of γ, and vice versa. As we will see later, this property leads to significant variations in the line shape with $R_\parallel$ if it survives in the real electronic structure. Our results suggest that this is possible only at small Z_t.

The panels Figs. 3(b) and 3(d) show the same as Figs. 3(a) and 3(c), but for a smaller wave vector $k_\omega = 0.6\,\text{Å}^{-1}$. Comparison between the right and left thus demonstrates the strong dependence of the substrate Green's function on the wave vector itself, not just the product $k_\omega R_\parallel$. The two most significant features are that, with decreasing k_ω, (1) the frequency and damping of the oscillations with $R_\parallel$ decrease, and (2) the dependence on Z_t weakens. In comparing the two different energies, we assumed that the damping constant λ (i.e., the tunneling barrier) is identical in the two cases. This would be the case in metals with identical work functions for states at the Fermi energy, in one of which the bottom of the band were closer to the Fermi level (smaller k_ω). We note that $k_\omega = 1.2\,\text{Å}^{-1}$ corresponds to an energy $\omega = 5$ eV in the middle of the parabolic band with our parametrization. Therefore, the value of $\Lambda(\mathbf{R}_t = 0) = 0$ at this energy, but is negative for smaller energies, e.g., for $k_\omega = 0.6\,\text{Å}^{-1}$, since in this case there are more high-energy continuum states repelling the discrete state downward than low-energy states pushing it up. We also see that the value of Λ at $R_\parallel = 0$ can change sign with Z_t depending on the energy ω. We note that, since Λ enters the expression for q, the Fano parameter, could also be negative and the asymmetry of the resonance line shape could be reversed.

F. Electronic structure effects and the surface states on (111) noble metals

In Sec. III E we introduced a simple model of G^+ based on the unperturbed jellium surface. In general, a more realistic behavior of G^+ can be obtained from electronic structure calculations. Here we qualitatively discuss the electronic structure effects with special attention to the (111) surfaces of noble metals frequently used in STM studies.

It is well known that (111) surfaces of noble metals contain Shockley surface states inside the projected two-dimensional band gap that forms on these surfaces.[52,53] Both the surface state and bulk wave function are given by the same general expression [Eq. (2.8)] outside of the metal surface. However, their overall degree of localization at the surface is determined by the position of ϵ_{ss}, the surface-state eigenvalue, with respect to the band-gap edges. All other things being equal, the most localized surface state occurs when ϵ_{ss} is at midgap. As ϵ_{ss} moves toward either band edge, the extension of the evanescent oscillatory tail of the surface-state wave function into the bulk increases, ultimately becoming identical to a periodic Bloch function when ϵ_{ss} hits the band edge. From elementary normalization considerations, surface-state extension into the bulk and amplitude at the surface, as reflected in the scale factor (or normalization constant) for the surface state tails [Eq. (3.27)] extending into vacuum, are intimately related; a greater population within the bulk means a lesser population in the surface region.[54,55] This surface-state delocalization into the bulk allows for the local density of bulk states at the surface to greatly exceed that of the surface states, in which case the relative importance of the surface state in the tunneling current will be small near the surface.[54] However, its importance increases with increasing distance from the surface, because bulk states with shorter wave-function tails are eliminated from the tunneling. The surface state accounts for about 50% of the total signal in typical STM tunnel junctions in Au(111),[56,57] and is known to be responsible for the interference effects observed on these surfaces near edges and impurities and in quantum corrals.[58–62] It will also play a disproportionately important role in the resonance tunneling at a large lateral tip-adsorbate distance, because its contribution to G_0^+ does not decay as quickly as that for the bulk states.

We see the different behavior of the bulk and the surface states in the STM when we consider the propagator G_0^+ for the Shockley state. This is again given by Eq. (3.29). How-

ever, the k sum now only extends over the two-dimensional (2D) wave vector $k_\parallel$. Assuming parabolic dispersion for the surface state, γ is given by

$$\gamma(\mathbf{R}_t,\omega)=J_0(k_\omega R_\parallel)e^{-\lambda Z_t k_\omega^2/2}, \tag{3.33}$$

and

$$\Lambda(\mathbf{R}_t,\omega)=\frac{1}{\pi\rho_s(\omega)}\int_0^{2D} d\epsilon\,\rho_s(\epsilon)\,\frac{\gamma(\mathbf{R}_t,\epsilon)}{\omega-\epsilon}, \tag{3.34}$$

where, as before, k_ω is the 2D wave vector of the substrate state corresponding to energy ω. The contribution of the Shockley state to the normalized density of conduction states $\nu(Z_t)$ is given by

$$\nu(Z_t,\omega)=e^{-\lambda Z_t k_\omega^2}. \tag{3.35}$$

The propagator G_0^+ for the surface state is thus essentially equal to the Bessel function $J_0(k_\omega R_\parallel)$ weighted by the exponential $e^{-\lambda Z_t k_\omega^2/2}$. Therefore, the oscillations are not damped with increasing Z_t and only their overall amplitude is diminished. Since the surface state on the noble metal surfaces (111) have a short $k_F\sim 0.15-0.2\,\text{Å}^{-1}$, its propagator will have a much longer spatial extent than that of the bulk states. The corresponding oscillations thus have a spatial period of about ten times that of the Bessel function J_0 in Fig. 3(a), in agreement with the experimental observation of DOS oscillations.

It is also known[56] that the spectral weight of the surface state decreases near surface imperfections. We expect the same to be true near the adsorbate. While we have explicitly taken into account the interaction of the conduction states with the discrete state a through the adsorbate Green's function G_a, all other adsorbate-metal interactions, such as potential scattering of the conduction electrons from the adsorbate and hybridization of the outer-shell adsorbate electronic states with the conduction electrons, are neglected in our model. In principle, these ''residual'' adsorbate-metal interactions can be included by modifying G^+ and t_{kp}. Although a realistic calculation of the system electronic structure is necessary to see the effect of the adsorbate on the behavior of G^+ around the adsorbate, we believe that it will not produce an oscillatory behavior in G^+. In a typical metal, several bands with anisotropic dispersion relations $\epsilon_{\mathbf{k}}$ contribute to G^+, giving rise to more complicated behavior. This will further reduce any oscillatory behavior seen in Fig. 3.

Since the importance of the direct tunneling into the tightly bound impurity orbital a relative to the tunneling into the metal should be weak, and decreases with increasing $R_\parallel$, it is useful to study the asymptotic behavior of the conductance $\mathcal{G}$ in the limit $t_a=0$. This is equivalent to replacing the Fano parameter $q(\mathbf{R}_t,\mathbf{R}_0;\omega)$ by $\Lambda(\mathbf{R}_t;\omega)$ inside $Y(\mathbf{R}_t,\mathbf{R}_0;\omega)$, [Eq. (3.23)] in the expression for conductance. It then follows that, if the oscillations in G^+ persist, the line shape should change with $R_\parallel$ and antiresonances should form at positions where $\Lambda^2>\gamma^2$. Using $G^+=\pi\rho_s e^{-Z/\lambda}(\Lambda-i\gamma)$ and

$$\begin{aligned}\mathrm{Im}\{G^+(\mathbf{R}_t,\mathbf{R}_0)G_a^R G^+(\mathbf{R}_0,\mathbf{R}_t)\}&\\ =-\pi^2\rho_s^2 e^{-2Z_t/\lambda}\{(\gamma^2-\Lambda^2)\,\mathrm{Im}\,G_a^R+2\Lambda\gamma\,\mathrm{Re}\,G_a^R\},&\end{aligned} \tag{3.36}$$

we can write $\Delta\mathcal{G}_{\mathrm{eq}}\equiv G_{\mathrm{eq}}-G_0$ at zero temperature by replacing $[-\partial f(\omega)/\partial\omega]$ by $\delta(\omega-V)$, and using $t_c(Z)=t_0e^{-Z/\lambda}$ as

$$\begin{aligned}\Delta\mathcal{G}_{\mathrm{eq}}(V)=&-\frac{2e^2}{h}t_0^2\rho_t(0)V_a^2\\ &\times\mathrm{Im}\{G^+(\mathbf{R}_t,\mathbf{R}_0;V)G_a^R(V)G^+(\mathbf{R}_0,\mathbf{R}_t;V)\}.\end{aligned} \tag{3.37}$$

We see that the resonance in the conductance is a result of an interference between different conduction states scattering resonantly from the impurity. Whether the resonance can be observed at large distances ($\geqslant 20$ Å) depends on the spectral weight of the surface state and on its hybridization ($\sim V_a^2$) with the impurity orbital a (usually d or f). Interesting spatial effects may be realized in system with suitable boundary conditions. We believe that Eigler's quantum mirage of the Kondo resonance inside the elliptical corral falls into this category.[63]

IV. DISCUSSION AND EXAMPLES

Equations (3.22) and (3.24) were derived under rather general assumptions. They are suitable as a starting point for numerical investigations given the necessary input from electronic structure calculations. In the rest of the paper, we discuss the implications of our theory for several specific cases of interest. In all of these cases we use our simple model for G^+ based on the jellium surface and the DOS given by $\rho_s(\omega)=\rho_t(\omega)=1-\omega^2/D^2$, with $D=5$ eV the band half-width. In order to eliminate the exponential fall-off in the tunneling conductance with the tip-surface separation and the background distortions, we plot the normalized change in conductance due to the additional impurity defined as

$$\Delta\mathcal{G}_{\mathrm{eq}}(V)\equiv h[\mathcal{G}_{\mathrm{eq}}(V)-\mathcal{G}_0(V)]/[2\pi e^2\rho_t(0)t_c^2], \tag{4.1}$$

where $\mathcal{G}_{\mathrm{eq}}$ is given by Eq. (3.24) and $\mathcal{G}_0$ by Eq. (3.25). This is equivalent to replacing Y by $\Delta Y=Y-\nu$ in the expression for $\mathcal{G}$.

Although we were motivated by the experimental observation of the Kondo resonance,[21,22] we discuss many of the tunneling properties on a simple noninteracting model. We do this primarily because most of the STM observable characteristics of the Fano resonance are common to the single particle and Kondo resonances, despite the difference in processes that give rise to the two resonances. We wish to point out these general features on a model that is conceptually far simpler and more familiar to the surface science community than the Kondo model, and emphasize that the resonances can also be observed in systems with nonmagnetic impurities with a tightly bound orbital near the Fermi level. Finally, the connection with Fano result and the consequences of the

spatial resolution of the STM become more transparent when the same noninteracting Anderson Hamiltonian is used.

A. Noninteracting adsorbate

We begin our discussion with an adsorbate-metal system described by the noninteracting Anderson model ($U=0$). The impurity resonance is characterized by its energy ϵ_0 and the width Γ_{as}. The retarded Green's function $G_a^R(\omega)$ for the adsorbate state is

$$G_a^R=(\omega-\epsilon_0-\mathrm{Re}\,\Sigma_a+i\Gamma_{as}/2)^{-1}, \tag{4.2}$$

where $\Gamma_{as}(Z_0,\omega)$ is defined in Eq. (3.14) and $\mathrm{Re}\,\Sigma_a(Z_0,\omega)=\mathcal{P}\Sigma_k|V_{ak}(Z_0)|^2(\omega-\epsilon_k)^{-1}$ is the real part of the self-energy for the noninteracting Anderson model [not to be confused with the real part of the substrate Green's function Λ given in Eq. (3.16)]. Following Fano, we now define the dimensionless energy parameter $\epsilon(\mathbf{R}_0,\omega)$ by

$$\epsilon=\frac{2(\omega-\epsilon_0-\mathrm{Re}\,\Sigma_a)}{\Gamma_{as}}. \tag{4.3}$$

We neglect all nonequilibrium effects, since they are likely to be insignificant for the noninteracting system under most experimentally realizable conditions. The differential conductance, in lowest order in t_c and t_a, is given by Eq. (3.24), where Y for the noninteracting system takes the form

$$Y\equiv Y_0=\nu+\frac{q^2-\gamma^2+2\epsilon\gamma q}{1+\epsilon^2}. \tag{4.4}$$

All terms are evaluated at energy ω and at the appropriate tip position. We note that $Y_0(0,0,\omega)\equiv Y_{00}$, characterizing the unphysical case of the STM tip in contact with the surface at the position of the adsorbate (embedded in the surface), has the analytic form obtained by Fano,

$$Y_{00}=\frac{(q+\epsilon)^2}{1+\epsilon^2}, \tag{4.5}$$

although the inherent energy dependence of q [through $\Lambda(\omega)$] could distort the pure Fano character of the line shape, even for this ''almost atomic physics'' STM example.

1. Line-shape dependence on electronic structure and on the relative strength of t_a and t_c

We first show (Fig. 4) the dependence of $\Delta\mathcal{G}_{\mathrm{eq}}$ on the ratio (t_a/t_c) for $\mathbf{R}_t=0$ and a resonance at the Fermi level. The solid line corresponds to a resonance at the center of a parabolic band (symmetric around its center), i.e., $\epsilon_0=5$ eV from the bottom of the band, and the dashed line corresponds to a resonance at $\epsilon_0=2$ eV from the bottom of the band. The two energies correspond to the band energy ϵ_k with wave vector $k=1.2\,\text{Å}^{-1}$ and $k=0.6\,\text{Å}^{-1}$ in our jellium model (Fig. 3). The resonance width is $\Gamma_{as}=0.2$ eV in both cases. At zero temperature, from Eqs. (3.24) and (4.4) we write

$$\mathcal{G}_{\mathrm{eq}}(V)=\frac{2e^2}{h}\rho_s(V)\,\pi\rho_t(0)t_c^2Y_0(V). \tag{4.6}$$

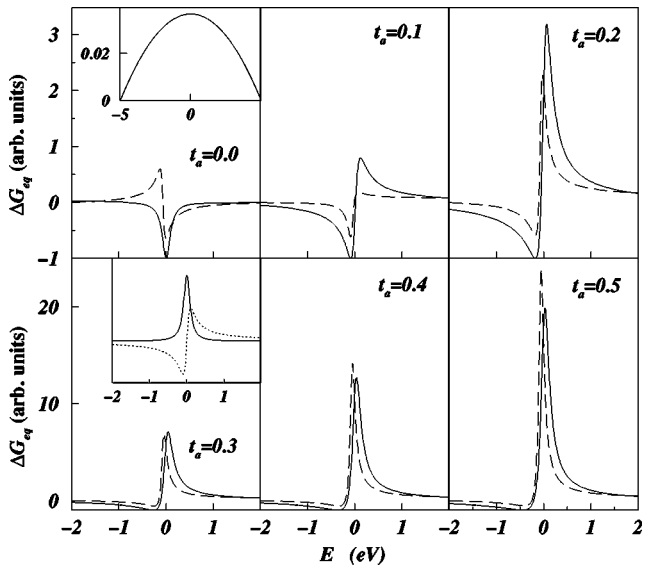

FIG. 4. Differential conductance $\Delta\mathcal{G}_{\mathrm{eq}}$ as a function of the strength of the direct tunneling matrix t_a (in units of t_c). The model parametrization is given in the text. The two curves correspond to two different impurity level energies $\epsilon_0=5$ eV (solid line) and 2 eV (dashed line) from the bottom of a symmetric band 10 eV wide. The two insets show the model density of states ρ_s for the conduction electrons (upper panel) and the imaginary (solid) and real (dashed) parts of $G_a(\omega)$ (lower panel).

In order to make connection with the Fano result, we plot the conductance for a small tip-metal separation with the tip above the adsorbate ($\mathbf{R}_t=0$). The line shape Y_0 is then given by the Fano formula [Eq. (4.5)]. The plotted quantity $\Delta\mathcal{G}_{\mathrm{eq}}(V)$ in Fig. 4 is then given by

$$\Delta\mathcal{G}_{\mathrm{eq}}(V)=\rho_s(V)\left(\frac{(q+\epsilon)^2}{1+\epsilon^2}-1\right). \tag{4.7}$$

The Fano parameter q depends not only on the ratio (t_a/t_c), but also on the energy and electronic structure. We see this most clearly in the first panel, where $t_a=0$. The resonance placed at the center of the band produces a symmetric dip in $\Delta\mathcal{G}$ characteristic of $q=0$, whereas the resonance at $\epsilon_0=2$ eV has an asymmetric line shape due to the negative contribution from Λ to q (see Fig. 3). Its line shape actually becomes symmetric at a finite value of t_a. The value of t_a inside each panel is given in units of t_c. The inset in the upper panel shows the model density of conduction states ρ_s, and the lower panel inset shows the spectral function $\rho_a=-(1/\pi)\mathrm{Im}\,G_a^R$ (solid line) and $\mathrm{Re}\,G_a^R/\pi$ (dotted line) for the level at the center of the band.

As the strength of the direct tunneling t_a increases with respect to t_c, the resonance develops its characteristic asymmetric shape and, eventually, at large $t_a/t_c\gg1$ it acquires a shape nearly indistinguishable from that of the impurity spectral function $\rho_a(\omega)$. With increasing tip-adsorbate separation, the signal from the resonance must disappear as both the tunneling element t_a and $G^+(\mathbf{R}_t,\omega)$ tend to zero. The differential conductance is then determined by the density of

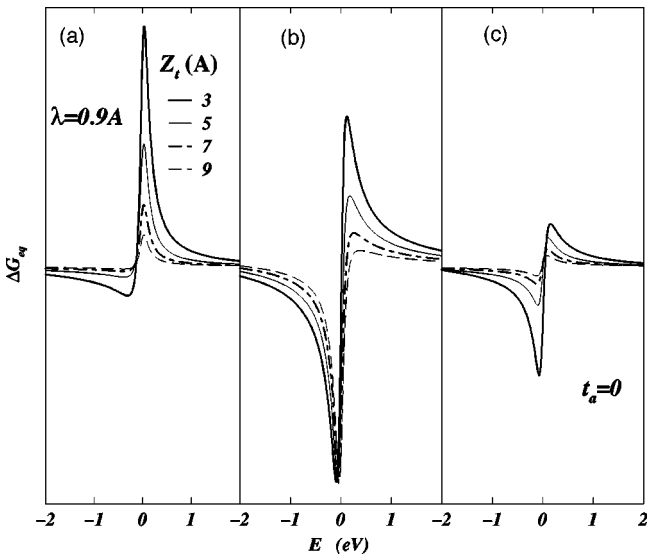

FIG. 5. Differential conductance $\Delta\mathcal{G}_{\rm eq}$ vs. Z_t for a model described in the text. (a) The complete dependence on the tip distance Z_t. (b) assumes $Z_t=0$ inside G^+, and thus neglects the wave-vector-dependent effects. (c) is the same as (a) but with $t_a=0$, i.e., it only includes the effect of decreasing spatial sensitivity incorporated through the substrate Green's function G^+. The vertical scale is arbitrary, but identical in all panels.

states of the clean surface. This property is not present in the Fano expression. We now discuss this behavior.

2. Line-shape dependence on the tip-surface separation

Using the same model system as in Sec. III, with the resonance at the center of the band ($\epsilon_0=5$ eV from the bottom of the band), we demonstrate the dependence on Z_t (with $\mathbf{R}_\parallel=0$) in Fig. 5. We make the following model for the tunneling matrix element $t_a(\mathbf{R}_t,\mathbf{R}_0)$ and $t_c(\mathbf{R}_t)$. The exponential fall-off of the metal and adsorbate wave functions is controlled by different decay constants. The adsorbate state ψ_a is tightly bound, especially for the narrow resonances of interest here. The conduction electron wave functions, on the other hand, typically belong to the outer *s* or *p* orbitals and have longer tails into the vacuum. As a consequence, the ratio t_a/t_c, and thus also the Fano parameter *q*, changes with Z_t. In order to incorporate this property, we use the matrix elements [Eq. (2.12)] and $t_c=t_0e^{-Z_t/\lambda}$, where $\alpha=0.75$ Å, $\lambda\approx0.9$ Å, $t_0=25$ meV, and $t_a=0.1t_c$ at $Z_t=2$ Å. Under these conditions, the *q* parameter tends to zero with increasing Z_t.

Figure 5(a) shows the normalized $\Delta\mathcal{G}_{\rm eq}$ for this model. The line shape undergoes only moderate changes with Z_t within the experimentally relevant range. We expect this to be a general property. In order to understand the behavior, we discuss the line-shape dependence on the tip-surface separation conceptually in terms of two contributions: (1) different decay constants for the discrete ψ_a and metal ψ_k states at the Fermi level, and (2) different decay constants for metal states at ϵ_{Fs} with different $k_\parallel$. We separate the observable consequences of these two effects in Figs. 5(b) and 5(c). The first contribution produces changes in *q* due to the changing relative strength between t_a and t_c. We demonstrate this in Fig. 5(b) where only this contribution is taken into account by setting $\gamma=\nu=1$ and $\Lambda=0$ in Eq. (4.4). This limit does not correspond to a real situation and does not lead to the correct $Z_t\to\infty$ limit. It is shown here merely as an example of the contribution [Eq. (1)] to the Z_t dependence of the tunneling conductance. With our parametrization, this case is identical with *q* changing from $q\approx0.8$ at $Z_t=3$ Å to $q\approx0.2$ at $Z_t=9$ Å. As Z_t increases further, $q\to0$ and the resonance becomes symmetric. However, we see that the normalized conductance $\Delta\mathcal{G}_{\rm eq}$ does not vanish in the limit $Z_t\to\infty$.

Figure 5(c) takes the second contribution [Eq. (2)] into account while leaving out the first one. We chose $t_a=0$, which would be the case if there were no direct tunneling into the discrete state. In this limit, any changes in the line shape are a consequence of the varying weight that different $k_\parallel$ metal states play in the tunneling at different Z_t's. This occurs because the $k_\parallel=0$ metal wave functions given by Eq. (3.28) have the greatest extension into the vacuum, and as a result the spatial resolution of the tip decreases. Therefore, the signature of the resonance in $\mathcal{G}$ decreases even after normalization of the current for different Z_t as the ratio $\Delta Y/\nu\to0$ with $Z_t\to\infty$. Figure 5(a) shows the combined effect of the contribution, and represents realistic conditions. It accounts correctly for the changing line shape, as well as its disappearance. We again emphasize that a realistic band structure is desirable for making quantitative statements.

It is clear that the line-shape dependence on Z_t will be observable only if it can be studied over a reasonably large range of Z_t, limited by the experimental resolution and detection capabilities. Since our model is based on realistic parametrization, we expect the behavior shown in Fig. 5 to serve as a guide for order of magnitude estimates for the spectral dependence on Z_t. The direct effect of the STM tip on the system, and thus also on the line shapes, is not taken into account here. This issue is discussed in Sec. IV B 3.

3. Line-shape dependence on the lateral tip position

As we discussed in Sec. III E, the resonance line shape depends on the relation between the spatial dependence of the direct tunneling and the propagation of the adsorbate-induced perturbation through the metal. Figure 3 shows that direct tunneling into the resonance (t_a) is expected to fall off faster than the perturbation. Therefore, at large $R_\parallel$, the line shape will be given by the $t_a=0$ limit conductance. We show the dependence of $\Delta\mathcal{G}_{\rm eq}$ on $R_\parallel$ in Fig. 6. We do this again for the model described in Sec. IV A 1 (Fig. 5) with $t_a=0$ and a resonance at the center of the band, i.e., $\epsilon_0=5$ eV from the bottom of the band, which corresponds to $k_\omega=1.2$ Å^{-1} in Fig. 3. The solid line corresponds to $Z_t=5$ Å, and the dashed line to $Z_t=0$ Å.

The unphysical case of $Z_t=0$ (dashed line) is shown to emphasize the possible consequence of the oscillations in G_0^+ displayed in Fig. 3. We chose the lateral tip positions in

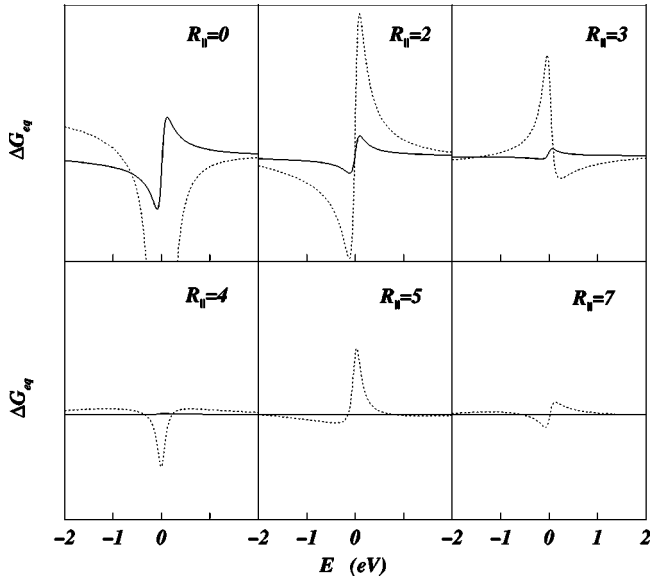

FIG. 6. The normalized differential conductance $\Delta\mathcal{G}_{\rm eq}$ as a function of the lateral tip position $R_\parallel$ for the same model as in Fig. 5: $Z_t=5$ Å (solid line) and $Z_t=0$ Å (dotted line). The contribution of the surface states to G_0^+ is not included here.

the figure to coincide with the nodes and zeros of Λ, and γ to show the dramatic changes in the line shape with $R_\parallel$ due to the oscillations in Λ and γ. Since the spatial decay of the oscillations is small at $Z_t=0$, the sequence of resonances and antiresonances appear in the range $R_\parallel \in (0,10)$ Å. The possibility for such antiresonances is discussed implicitly in the work of Kawasaka *et al.*,[49] and explicitly by Schiller and Hershfield.[64] However, this behavior is not observed in the experiments by Madhavan *et al.*[21] and Li *et al.*[22] due to the smoothing of the electronic structure with increasing distance from the surface that we discussed in Sec. III E.

In fact we would not expect the dramatic variations in line shape with $R_\parallel$ reported by Schiller and Hershfield[64] to be observed. The reason is apparent from the behavior of G^+ as a function of Z_t (Fig. 3). As the distance from the tip to the surface increases, the oscillations are destroyed by the increasing weight of the lower frequency (small $k_\parallel$) components at larger Z_t interfering destructively with those given by k_ω. For $k_\omega=1.2\,\text{Å}^{-1}$, the oscillations are effectively damped when $Z_t \geqslant 5$ Å, and the shape of the resonance does not change significantly as shown by the bold line in Fig. 6. We expect that band-structure effects will suppress the oscillations even further.

We also find that the spatial extent of the resonance in the spectrum should decrease as the STM is retracted, as long as the signal is due to the bulk states. At $Z_t=0$ Å, the resonance is still visible at $R_\parallel \sim 10$ Å but only to about $R_\parallel \sim 4$ Å at $Z_t=5$ Å. This is a somewhat shorter distance than that found experimentally for Co/Au(111) and Ce/Ag(111).[21,22] Although the Fermi wave vector $k_F \approx 1.2\,\text{Å}^{-1}$ used in Fig. 6 is close to the free-electron value of k_F for the noble metals, the disagreement is not surprising since we made no real attempt at realistic electronic structure description. Smaller values of k_F would increase the spatial extent as would smaller values of Z_t and λ.

Interestingly, the $Z_t=0$ (dotted line) line shape progression shown in Fig. 6 is qualitatively similar to the family of line shapes that would be expected from surface state propagation, but with $R_\parallel$, the lateral tip-adatom separation rescaled upward by nearly an order of magnitude. This claim is based on the qualitative similarity between the bulk G_0^+ at $Z_t=0$ and the surface G_0^+. The bulk $\gamma(R_\parallel,\epsilon_F)=j_0(k_F R_\parallel)$ (the dashed curve in Fig. 3) at $Z_t=0$ and the analogous surface state $\gamma(R_\parallel,\epsilon_F)=J_0(k_F R_\parallel)$ (dotted curve in Fig. 3) both exhibit long-range oscilla-tions, unlike the bulk state at $Z_t \geqslant 5$ Å. However, since $k_F \sim 0.1-0.2\,\text{Å}^{-1}$ for the surface-state band, $J_0(k_F R_\parallel)$ shown in Fig. 3(a) for $k_F=1.2\,\text{Å}^{-1}$ should be plotted with this smaller k_F when referring to actual noble metal surface state bands, in which case the observable $R_\parallel$-dependent line-shape evolution in Fig. 6 would still be representative, but with $R_\parallel$ rescaled by the factor 1.2/0.15 $=8$. From this it is easy to appreciate that the dramatic line-shape variations will occur mainly at very large lateral separations.

B. Tunneling into Kondo resonance

In Sec. IV A, we discussed the STM conductance in tunneling through a noninteracting impurity [$U=0$ in Hamiltonian (2.1)], frequently referred to as the resonant level model (RLM). We now turn to the case of magnetic impurities and tunneling through a Kondo resonance. We begin with the case of a weak tip-metal coupling. However, for the Kondo systems this assumption is more restrictive than for the RLM, and, for this reason, we later take advantage of our nonequilibrium approach to account for the direct effect of the tip on the impurity spectral density, while still neglecting the tip's effect on the metal states.

1. Conceptual and theoretical approach

Since our earlier derivation of the current and conductance is valid for arbitrary interaction [$U\neq 0$ in Eq. (2.1)], the final results [Eqs. (3.22) and (3.24)] also hold in the Kondo and mixed-valent regimes of the Anderson model (i.e., $U \gg \Delta$). The properties of the adsorbate enter through the Green's function G_a. The problem is thus reduced to finding the one-electron Green's function G_a.

However, we first consider the tunneling for a spin-$\frac{1}{2}$ ($a \equiv \sigma$) impurity in the Kondo limit, $(\epsilon_{Fs}-\epsilon_0) \gg \Gamma$ and $(\epsilon_0 - \epsilon_{Fs}+U) \gg \Gamma$. The Kondo resonance has a very small weight, and is due to spin fluctuations. The possible tunneling channels in this case are shown in Fig. 7 as processes (1) and (3). The system can be described by the Kondo Hamiltonian in this limit

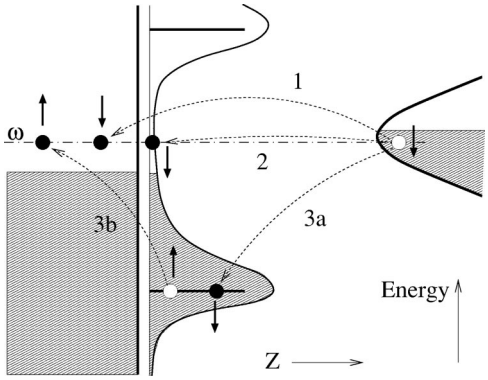

FIG. 7. Possible scattering channels for an electron tunneling from tip to metal through a magnetic impurity adsorbed on the surface.

$$H_s(Z_0)=\sum_{k\sigma}\epsilon_k c^\dagger_{k\sigma}c_{k\sigma}+\sum_{p\sigma}\epsilon_p c^\dagger_{p\sigma}c_{p\sigma}$$
$$+\sum_{kp\sigma}\{t_{kp}(\mathbf{R}_t)c^\dagger_{k\sigma}c_{p\sigma}+\text{H.c.}\}$$
$$+J_s\sum_{kk'\sigma\sigma'}(c^\dagger_{k\sigma}\mathbf{s}_{\sigma\sigma'}c_{k'\sigma'})\cdot\mathbf{S}$$
$$+J_t\sum_{pp'\sigma\sigma'}(c^\dagger_{p\sigma}\mathbf{s}_{\sigma\sigma'}c_{p'\sigma'})\cdot\mathbf{S}$$
$$+J_{st}\sum_{kp\sigma\sigma'}\{(c^\dagger_{k\sigma}\mathbf{s}_{\sigma\sigma'}c_{p\sigma'})\cdot\mathbf{S}+\text{H.c.}\},\quad(4.8)$$

where the first three terms were also present in the total Hamiltonian introduced in Sec. II and describe the unperturbed metal and tip states and the coupling between the two. The remaining terms give rise to spin fluctuations in the presence of the magnetic impurity. The terms with couplings J_s and J_t correspond to the exchange interaction of the local spin with the substrate and tip electrons, respectively. The last term (J_{st}) corresponds to the effective tip-substrate exchange interaction in which charge is transported between the tip and the surface. This Hamiltonian can be obtained from H_{tot} of Sec. II using the Schrieffer-Wolf transformation which relates J_s, J_t, and J_{st} to V_a and t_a. For the symmetric Anderson model, $J_s=4V_a^2/U$, $J_{st}=4t_aV_a/U$, and $J_t=4t_a^2/U$. Using the continuity equation (3.1), the current is

$$I=\frac{2e}{\hbar}\text{Im}\Bigg\{\sum_{kp\sigma}t_{kp}\langle c^\dagger_{k\sigma}c_{p\sigma}\rangle+J_{st}\sum_{kp\sigma\sigma'}\langle c^\dagger_{k\sigma}\mathbf{s}_{\sigma\sigma'}c_{p\sigma'}\cdot\mathbf{S}\rangle$$
$$+J_t\sum_{pp'\sigma\sigma'}\langle c^\dagger_{p\sigma}\mathbf{s}_{\sigma\sigma'}c_{p'\sigma'}\cdot\mathbf{S}\rangle\Bigg\}.\quad(4.9)$$

The first term is identical with the first term in Eq. (3.3). In the lowest order of the tip-system couplings (t_{kp}, J_{st}, J_t), the third term does not contribute. The first term corresponds to the direct tip-substrate tunneling channel—process (1) in Fig. 7—which includes the scattering of conduction electrons from the local moment. The second term corresponds to the direct tunneling into the magnetic impurity—process (3) in Fig. 7. We note that the spin-flip scattering that gives rise to the Kondo effect is a higher-order process. In lowest order, channel (1) and the spin-flip component of (3) do not give rise to interference because the final states have different spin states. The lowest spin-flip process that does interfere with (1) is of second order in J and proportional to J_sJ_{st}.

In the limit of large tip-metal separation, equivalent to the condition ($J_s\gg J_{st}\gg J_t$), the third term in Eq. (4.9), as well as higher-order contributions from J_{st}, are neglected, and all other exchange processes are included in principle. This is equivalent to assuming that the state of the metal-adsorbate system is determined only by J_s, and is unaffected by the presence of the tip. Theoretically, the problem then reduces to finding the spectral properties of the system without the tip and using them in the expansion for tunneling via the two terms in Eq. (4.9).

As the system parameters move away from the Kondo limit—that is either ϵ_0 shifts toward ϵ_{Fs} or U becomes smaller—valence fluctuations appear. The Kondo resonance is then due to both the spin and charge fluctuations. The separate energy scale due to the spin fluctuations eventually disappears in the mixed-valent regime, and the Kondo peak merges with the broad resonance centered at ϵ_0. In the intermediate regime, where both charge and spin fluctuations coexist on the impurity, another tunneling channel exists. This channel is denoted by (2) in Fig. 7. It also includes the contribution from higher-order nonflip processes similar to (3). We study the system in this regime with the Hamiltonian defined in Sec. II.

We adopt the slave-boson technique of Coleman,[65] and find the adsorbate Green's function using the noncrossing approximation (NCA).[13] Following the theory of Sec. III, the final expression for current in Eq. (3.4) is valid, as well as all the consequent steps and approximation in Sec. III. We insert the solution for the Green's function G_a of the ($U=\infty$) interacting system in Eq. (3.24). This is equivalent to including the three tunneling channels in Fig. 7 to lowest order in the tip-system couplings. We now turn to the discussion of the results based on this approach.

2. Results for large tip-substrate separation

In order to model Co/Au(111), studied both experimentally[21] and theoretically,[49] we choose a parametrization that gives the Kondo temperature $T_K\approx 70$ K appropriate for the system. Our simplified model has degeneracy $N=2$ with no orbital degeneracy, bandwidth $2D=10$ eV, and an adsorbate level at $\epsilon_0=0.75$ eV with a width $2\Gamma=1$ eV (the width of a multiplet with an occupied level is $N\Gamma$ rather than Γ). We show the corresponding spectral function and the real part of G_a in the inset of Fig. 8.

Figure 8 shows the spectral properties of the system using $\Delta\mathcal{G}_{\text{eq}}$ over the whole energy range of the conduction band, and for different values of q at the Fermi level. The spectrum contains information about the broad resonance at $\epsilon_0=0.75$ eV below the Fermi level, as well as the prominent feature due to the Kondo resonance at zero bias. We show the large bias voltage results only for completeness, since we

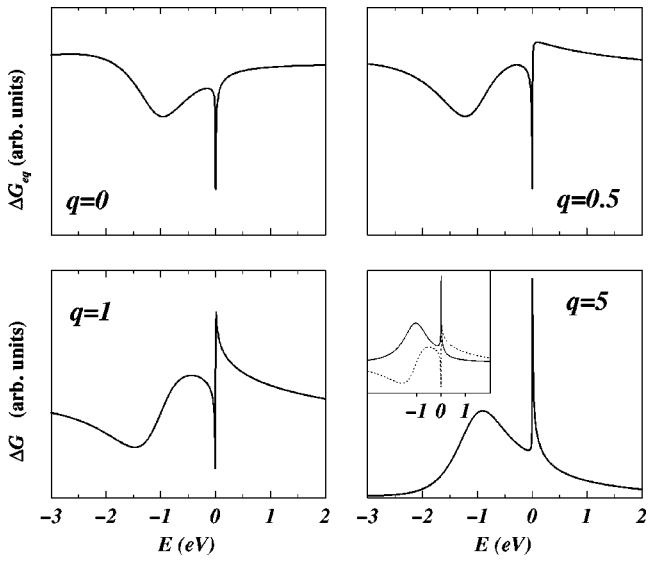

FIG. 8. The spectral line shape for a model Kondo system described in the text over a large bias range that includes tunneling into the broad resonance at 0.75 eV below the Fermi level. Each panel corresponds to different $q(\epsilon_{Fs})$ at the Fermi level.

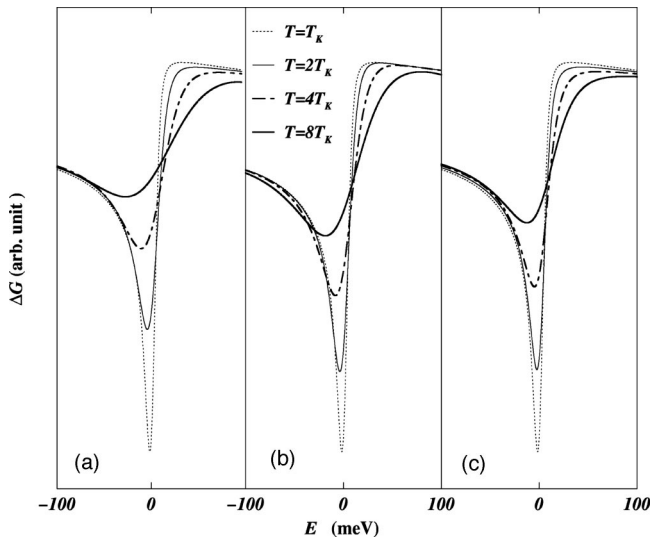

FIG. 9. Temperature dependence of the tunneling conductance through the Kondo resonance. (a) The total dependence includes the temperature dependence in the spectral function and the Fermi-surface broadening. (b) Temperature dependence due to the Fermi-level broadening, and with a spectral function given by its $T \approx T_K$ value for all temperatures. (c) Temperature dependence of only the spectral function, without the Fermi-surface broadening (replaced by a delta function).

do not expect the STM experiments to be able to provide spectroscopic information about the system over the whole energy range shown.

The resonance line shapes in both Co/Au(111) and Ce/Ag(111) correspond to small values of q. Madhavan *et al.*[21] fitted the observed resonances to Fano line shapes with $q \sim 0.7$. Our best fit would give approximately the same value of q. In the case of Ce/Ag(111), the observed feature is an almost symmetric antiresonance corresponding to $q \sim 0$. Due to the contribution from the substrate electronic structure to q, its value cannot be directly used to make quantitative statements about the relative strength of the tunneling into the discrete state d (f) with respect to that into the continuum. However, in agreement with Li *et al.*[22] and Lang,[66] we conclude that the STM probes mostly the *sp* wave functions and the tunneling into the *f* orbital is rather weak at the tip-adsorbate distances used in the Ce/Ag(111) experiment. The resonance is mostly the result of interference between conduction electrons scattering from the impurity. The larger value of q in Co/Au(111) indicates a stronger contribution from the coupling of the STM to the d orbital. This is expected because the $3d$ orbital is not as tightly bound.

The recent work of Kawasaka and co-workers[48,49] deals with the spatial and spectroscopic profiles of the Kondo resonance. They began with the Tersoff-Hamann[24] expression for the current [Eq. (3.11)], and used the local density of states given by Eq. (3.13). They inserted the self-energy correction in the Green's function G_a due to the intra-adsorbate Coulomb correlations using perturbation theory ($T > T_K$) and Yamada's expansion in U ($T < T_K$) to study the temperature dependence in the whole temperature range. They neglected the additional temperature effects due to the Fermi surface broadening, replacing $(-\partial f/\partial \omega)$ by the delta function, and evaluated the conductance at the tip bias.

One of the main conclusions of their work[49] is that the calculated temperature dependence of the resonance in the differential conductance is indicative of the temperature dependence of the Kondo resonance itself. They showed results at the experimentally relevant low temperatures for Co/Au(111) and Ce/Ag(111) in the range of temperatures ($T \leqslant 0.1 T_K$). They found a rather weak temperature dependence, due entirely to the temperature dependence of the spectral function ρ_a. It is qualitatively the same as, and comparable in magnitude with, that found in Fig. 9(b), where the spectral function is independent of temperature and the temperature dependence in $\Delta \mathcal{G}_{\rm eq}$ is the consequence of the Fermi-surface broadening in the STM tip. Therefore, a careful deconvolution is necessary even at these low temperatures to extract information about the temperature dependence of the Kondo resonance. The other possibility is to eliminate variations in the Fermi-surface broadening of the tip.

We show the temperature dependence for a Kondo system in Fig. 9. Since the validity of our approximation is limited to temperatures of order T_K and higher, we show our results only in this temperature range. Figure 9(c) shows the temperature dependence one would observe with the tip at $T = 0$ K and with a varying substrate temperature, i.e., when only the temperature dependence of the spectral function is taken into account. Figure 9(b) assumes the substrate is at a constant temperature $T = T_K$, which determines the shape of the Kondo resonance, while the tip temperature is varied. We see that the two contributions produce a very similar broadening of the Fano resonance. Only a close look can uncover the difference. Figure 9(a) shows the combined effect when the tip and substrate are kept at a common temperature. Ob-

viously, it would be difficult to determine the contribution from the broadening of the Kondo resonance.

In addition to the temperature effects just discussed, Kawasaka and co-workers[48,49] also predicted the existence of weak, long-range oscillations in the current as a function of the lateral tip position. The particular long-wavelength, long-range character of these predicted oscillations is a consequence of their assumption that the tip-to-metal tunneling takes place into the surface states of the (111) noble metal surfaces. The observed resonances[21,22] are at variance with these expectations. On the other hand, the limited spatial extent of the resonance observed at lateral tip positions up to 10 Å is consistent with the rapid spatial decay determined by the bulk G_0^+. No significant changes in the resonance line shape are expected on this length scale (see the discussion in Sec. III F, and Fig. 6). The surface state would, however, be responsible for line-shape variations on larger length scales of order 20 Å. The fact that no resonance is observed at such a distance from the impurity indicates that the surface-state contribution is indeed weak. Since Friedel oscillations have been observed over long tip-impurity separations, we believe that a weak tunneling resonance most likely persists in the conductance over comparable distances, but more sensitive experiments are necessary. In this case, changes in the line-shape with $R_\parallel$ are expected. However, unlike Schiller and Hershfield,[64] we do not expect variations in the line shape due to the dominant contribution from the bulk states on the length scale of $\leqslant 5$ Å, as discussed in Sec. IV A 3.

3. Nonequilibrium and hybridization effects at small tip-substrate separation

In typical STM experiments, the tip-substrate separation can be varied from the point of contact where the tunneling resistance R is a few 100 kΩ to distances where $R \sim 1$ GΩ. Experimental constraints limit the STM usefulness to the near-Fermi-level spectroscopy—especially at small Z_t—because of exponentially increasing tunneling currents with bias. However, it is likely to be possible to investigate the Kondo resonance—which only requires biases of the order of ~10 meV—with very small tip-adsorbate separations. It is therefore useful to analyze the physical consequences of the small tip-metal separation on the resonance in tunneling conductance.

In this case, nonequilibrium effects, as well as the tip-adsorbate interaction, become important in the spectroscopy of Kondo systems. First of all, as Γ_{at} increases and becomes a significant fraction of Γ_{as} at small distances, the tip-adsorbate hybridization will contribute to the width Γ of the resonance and to the renormalization of the level ϵ_0. As a result, the Kondo temperature, which depends sensitively on Γ and ϵ_0, will change. This could be particularly important for systems with very low bulk T_K, such as Fe/Au with $T_K \sim 1$ K. The Kondo temperature for an impurity adsorbed on the surface of the metal is even lower than its bulk T_K because the lower coordination number for the adsorbate makes the width Γ narrower. If $T_K \ll T$, the Kondo resonance will not be observed. In certain systems and in the right temperature regime, it may be possible for the Kondo resonance to reappear at smaller tip-adsorbate distance as a result of the increased hybridization. This could also be achieved by incorporating the adsorbate into the top surface layer. The recent study of transition-metal impurities at the surface of gold[67] did not find any sign of the Kondo effect in V, Cr, Mn, or Fe. We believe that, in the case of iron, this is due to the low T_K, and may be an example of a candidate system for the conditions discussed here. On the other hand, the smaller impurity-metal hybridization at the surface can lead to magnetic behavior for systems which are nonmagnetic in the bulk, such as Ni/Cu. There is a possibility for observing the transition between magnetic and nonmagnetic behavior on a single system induced either by embedding or by the proximity of the STM tip.

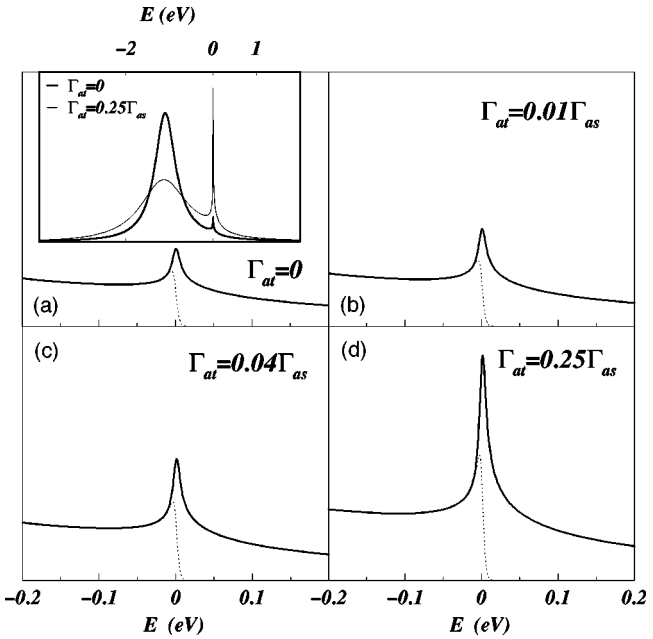

FIG. 10. The spectral function $\rho_a(\omega)$ at zero bias as a function of the tip-substrate separation (defined in terms of Γ_{at}). Dotted line, occupied density of states; bold line, spectral density of states.

We show an example of the changing T_K with hybridization in Fig. 10, where the spectral function $\rho_a(\omega)$ is plotted at zero bias as a function of the partial width Γ_{at}, i.e., the tip-metal separation for a model system. We choose $D = 5$ eV, $\Gamma_{as} = 0.25$ eV, $\epsilon_a = -1$ eV, and $T = 30$ K. The Kondo temperature for this model in the limit $t_a = 0$, is $T_K \sim 30$ mK, much smaller than the temperature T. Therefore, the Kondo resonance in the spectral function is very weak. When the tip is brought closer to the adsorbate, the Kondo resonance acquires more spectral weight as the Kondo temperature increases to $T_K \sim 100$ mK at $\Gamma_{at} = 0.01\Gamma_{as}$, $T_K \sim 0.2$ K at $\Gamma_{at} = 0.04\Gamma_{as}$, and $T_K \sim 1.5$ K at $\Gamma_{at} = 0.25\Gamma_{as}$. Based on the justifications in Appendix A, we neglected the effect of the direct metal-tip interaction on the spectral function, and treat the effect of the tip as another hybridization channel for the impurity state.

The effect of varying hybridization—due either to the presence of the STM tip or to embedding or changing the environment of the adsorbate—on the tunneling resonance depends on the relation between T_K and T. For instance, when $T_K \ll T$, increased hybridization would produce stron-

ger (sharper) tunneling resonance of the same width since the spectral weight in the Kondo resonance increases while its width remains almost constant until $T_K \sim T$. Also, the experimental resolution is limited by temperature in this regime. When, on the other hand $T_K \geqslant T$, additional hybridization would not only increase the spectral weight in the Kondo resonance but also its width. The two cases should thus be distinguishable experimentally from each other and from the possible line-shape variations with Z_t as a result of changing q.

The second important effect of the strong tip-adsorbate interaction is the breakdown of equilibrium relations at finite bias such as the fluctuation-dissipation theorem $G^<(\omega) = f(\omega)\rho_a(\omega)$, which consequently cannot be used in deriving the expression for the current [Eq. (3.22)]. This is true in general because the electron occupation of the tip, metal, and adsorbate electrons will no longer be thermal, i.e., will not be given by $f_t(\omega)$ and $f_s(\omega)$ but rather will be characterized by a nonequilibrium distribution produced by the injected tunnel electrons. The differential conductance is no longer proportional to the local density of states, and cannot be obtained using Eq. (3.24). In Kondo systems, the hot electrons not only modify the electronic distribution on the impurity, but also modify the Kondo resonance itself.

This is shown Fig. 2, where the spectral function and density of occupied states is plotted at selected bias voltages in the limit of $|t_{pk}| \ll |t_{pa}|$. The impurity has a resonance at $\epsilon_0 = -1$ eV below the Fermi level, and a total width $\Gamma = 0.5$ eV produced by hybridization with both the tip and substrate with partial widths of $\Gamma_{at} = 0.1\Gamma_{as}$. The temperature is of the order of T_K in this example. We see that the Kondo resonance broadens even more with increasing bias. This is due to the increase in the rate of incoherent scattering by $\sim eV_a/T$—an effect similar to temperature. At the same time, the electron occupation develops a nonthermal profile due to the large tip-adsorbate current. This is particularly visible for negative biases where the density of states is larger. Figure 2(a) shows the equilibrium spectral function (dotted line) and the electron population on the resonance (solid bold line). The equilibrium spectral density is shown (dotted line) in all panels. In addition, the spectral density (solid line) and occupation (bold solid line) are shown for the biases indicated in the figure by the labeled arrow. If the coupling to the tip were comparable with the metal-adsorbate hybridization, a double-peak structure would develop. This was predicted by Wingreen and Meir[50] in the context of the nonequilibrium Kondo effect in quantum dots, also discussed in Ref. 68. We see the onset of the double peak structure in Figs. 2(b)–2(d), where a small cusp develops at the chemical potential of the tip. In summary, the bias has a significant effect on the spectral density even when $\Gamma_{at} \sim 0.1\Gamma_{as}$.

We show the tunneling current (right) and the corresponding differential conductance (left) in Fig. 11 for this model of Kondo impurity and for the STM geometry defined by $\Gamma_{at} = 0.1\Gamma_{as}$ and $|t_{pk}| \ll |t_{pa}|$. The panels correspond to $q = 0.6$, 1.2, and 2.4, respectively. The current on the right is calculated using $I_{\rm tot} = I_{\rm eq} + \delta I_{\rm non}$ of Sec. III D, with $\delta I_{\rm non}$ given by Eq. (3.26). The differential conductance $\mathcal{G}_{\rm tot}$ on the left is obtained by differentiating the results displayed on the right.

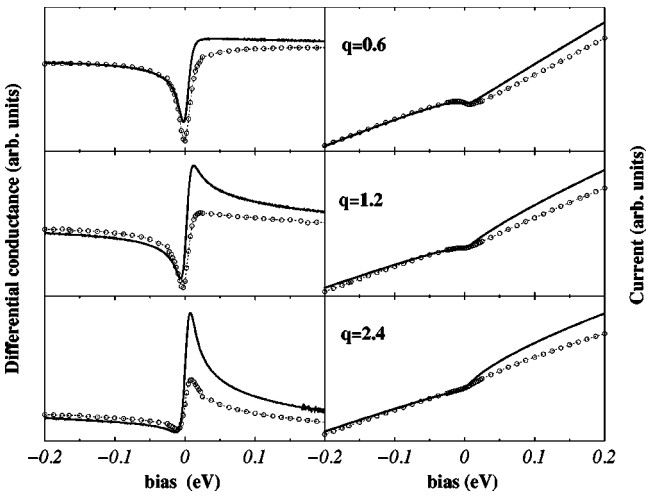

FIG. 11. Differential conductance (left) and current (right) for a Kondo system defined in the text and with the spectral function displayed in Fig. 2. The solid line is a calculation at lowest order in t_{kp} and t_{ap}, and with an equilibrium spectral function of Fig. 2. Circles correspond to the nonequilibrium $\mathcal{G}_{\rm tot} = dI_{\rm tot}/dV$ and $I_{\rm tot}$ for $\Gamma_{\rm at} = 0.1\Gamma_{as}$. Each row corresponds to a given value of q at the Fermi level.

It cannot be calculated from the expressions in the text, since the dependence of $\rho_a(\omega)$ and $G_a^<(\omega)$ on the bias voltage modifies the contributions to the current in a wide energy range, and $\mathcal{G}_{\rm tot}$ is not related in simple terms to the properties at the Fermi level of the tip. We compare $I_{\rm tot}$ and $\mathcal{G}_{\rm tot}$ (circles) with $I_{\rm eq}$ and $\mathcal{G}_{\rm eq}$ (solid). The equilibrium quantities were obtained in the lowest order in t_{ap} and t_{kp}, and with the equilibrium G_a of Fig. 2(a).

We see that the broadening and disappearance of the Kondo resonance with increasing bias at strong tip-adsorbate coupling is weakened in the nonequilibrium calculation of $\mathcal{G}_{\rm tot}$, because the contribution $\delta I_{\rm non}$ compensates partially for the spectral function effect. The most consistent effect on the line shape for various values of q is the suppression of the resonance maximum, and as a consequence of this the line shape has a more symmetric appearance. This behavior is qualitatively different from both the hybridization effect and that of the changing Fano parameter q—due to different decay constant of the impurity and metal states. Although the dependence of the tunneling resonance on the tip-substrate separation Z_t will contain all three contributions, the hybridization and nonequilibrium contributions should only be important at extremely small tip-adsorbate separations. The variations in q should not be important as it depends on the difference of the wave-function tails, and the two remaining contributions should leave distinguishable signatures in the tunneling resonance. It remains to be seen if the nonequilibrium condition play an important role in the tunneling between the STM tip and the Kondo impurity.

Finally, we note that the limit $|t_{pk}| \ll |t_{pa}|$ discussed here in connection with the nonequilibrium effects is not appropriate for the recent STM experiments, where t_{pa} is likely much weaker than t_{pk}, even though the importance of t_{pa} will increase relative to t_{pk} with decreasing Z_t. We will address the more general case in a future work.

V. CONCLUSIONS

We used the Keldysh-Kadanoff method to study the spectroscopic features of adsorbate resonances in the STM tunneling experiments. The central results of our theory are the general expression for the current [Eq. (3.4)] to all orders in the tunneling matrix elements and its equilibrium limit [Eq. (3.10)]. Both are valid for arbitrary intra-adsorbate electron correlations, and thus apply to both noninteracting ($U=0$), as well as magnetic (large U) systems. The discussion of the Fano resonances is based on additional approximations for the tunneling and hybridization matrix elements that lead to expressions (3.22) for the tunneling current and Eq. (3.24) for differential conductance in the lowest order in the tip-to-system tunneling matrix elements t_a and t_c, i.e., at a large tip-surface separation, and the nonequilibrium correction to the current in Eq. (3.26).

In the equilibrium limit, our theory of the tunneling current and conductance differs from the standard theories of STM, in that the dependence on LDOS is replaced by a tip-specific quantity related to the LDOS [Eq. (3.9)]. The current is expressed entirely in terms of the adsorbate Green's function G_a^R, the tip density of states, the tunneling matrix elements, and the substrate Green's function. We used the formulation to study the resonance line shape as a function of temperature, tip-substrate separation, and lateral tip position. We summarize our findings as follows.

(1) The role of impurity state resonances in tunneling can be discussed in terms of two limiting cases. When direct tunneling across the barrier is weak, the resonance within the barrier provides an additional tunneling channel and can significantly enhance the tunneling current. This is the case of quantum dots in Coulomb blockade regime. If on the other hand, the tunneling into the continuum is strong, the presence of an ''impurity'' state could suppress the tunneling current due to the additional scattering of the conduction electrons in the metal from the impurity, i.e., increased resistance. The tunneling into the Kondo resonance in the recent STM experiments seems to be closer to the latter limit.

(2) The information about electron correlations and the Kondo resonance enters the tunneling problem through the impurity Green's function G_a while the position dependence of the conductance is controlled by the electronic structure of the metal.

(3) The spatial decay of the observed Fano resonance in the recent experiments[21,22] is consistent with the conclusion that tunneling into the bulk conduction and hybridized sp impurity states gives rise to most of the signal. The absence of any observable resonance at distances larger than ~ 10 Å suggests that the contribution from the surface state on Au(111) and Ag(111) to the resonant tunneling is not important in these experiments. However, the surface states are important in special cases, as indicated by the recent corral experiments[63] in which the contribution of the surface states is enhanced by scattering from the walls of the corral.

(4) At large Z_t, tunneling into conduction states with $k_\parallel$ having the smallest parallel component corresponding to energy $\omega=\epsilon_{k_\perp}+\epsilon_{k_\parallel}$ is strongly favored. This leads to the disappearance of the current oscillation vs the lateral tip position due to tunneling into the bulk states which should otherwise be observed with period of about 1–2 Å (corresponding to the bulk k_F) for typical experimental conditions. Therefore, no oscillations in the line shape should be observed on this length scale for typical tip-surface separation. The occurrence of an antiresonance with tip position at certain neighboring sites predicted by Schiller and Hershfield[64] has its origin in these oscillations. It is a result of a simplified model for the surface electronic structure and we believe it is unphysical. The small current oscillations predicted by Kawasaka *et al.*[49] assumed that the surface states are all-important in the spatial dependence of the resonance which seems to contradict the experimental results. We believe the surface state should be important at larger distances since on the (111) noble metal surfaces $k_F \sim 0.15-0.2\,\text{Å}^{-1}$ and the corresponding period of oscillations is about 20 Å (as observed experimentally as Friedel oscillations). We expect changes in the resonance line shapes with this spatial period if the contribution is from the surface state and if the signature of the resonance is detectable at such distances.

(5) From the line shapes observed in Co/Au(111) and Ce/Ag(111), we conclude that the direct tunneling into the discrete (d or f) state is quite weak—stronger in Co/Au(111). This confirms that the STM is mostly a probe of the delocalized sp states and couples only weakly to the tightly bound d or f orbitals at typical tip-surface separations. Therefore, the dominant process giving rise to the resonance line shape is the tip-to-metal tunneling and interference between conduction electrons scattering from the local moment.

(6) The temperature dependence in differential conductance does not reflect only the temperature dependence of the Kondo resonance, but also includes the effect of Fermi-surface broadening (mostly of the tip). The two contributions are of the same order of magnitude, and qualitatively indistinguishable. Therefore, the temperature dependence in the differential conductance cannot be used directly to make conclusions about the temperature dependence of the resonance without controlling the tip Fermi-surface broadening or without deconvolution.

(7) At small tip-surface separations, nonequilibrium effects as well as the additional tip-adsorbate hybridization may play an important role—especially in Kondo systems. The main effect of the finite bias voltage in this case is to broaden the Kondo resonance and produce a nonequilibrium electron population on the adsorbate. The observed Fano resonance in differential conductance also broadens and its maximum is suppressed. The effect of the tunneling current on the Kondo resonance should thus leave a characteristic dependence of the line shape on Z_t.

Note added. Since the submission of this manuscript we have learned of related work by Újsághy *et al.*[69]

ACKNOWLEDGMENTS

We thank R. Celotta, E. Hudson, M. Stiles, and J. Stroscio for fruitful discussions, and for helping us understand the experimental issues more clearly.

APPENDIX A: ADSORBATE GREEN'S FUNCTION

An important quantity in the theory of tunneling current through adsorbate resonances is the adsorbate Green's function G_a. Using the equation-of-motion method, we find the expression for G_a defined as the Fourier transform of

$$G_a(t,t') = -i\langle T_C c_a(t) c_a^\dagger(t')\rangle. \tag{A1}$$

We do this for the case of arbitrarily strong coupling between the tip and the adsorbate, with the intent of describing the nonequilibrium effects at finite bias. However, in this paper we consider the effect of the direct tip-metal interaction on G_a to be weak, and neglect it. Extension to the full description will be considered in future work. We believe the approximations adopted here capture the most important nonequilibrium effects.

We discuss both the noninteracting ($U=0$) and interacting ($U=\infty$) models. Since the solution in both limits for the adsorbate-metal interaction is well known, we limit our discussion to issues specific to the addition of the biased tip, and refer the reader to standard texts for details. The ($U=\infty$) model is solved using the slave-boson technique and the NCA. In this approach a pseudofermion is introduced by the transformation $c_a \rightarrow c_a b^\dagger$ in the Hamiltonian (2.1), where $b^\dagger$ is the creation operator for the slave boson. This eliminates the interaction term U from the Hamiltonian as discussed by Coleman.[65]

The time-ordering operator T_C orders the time according to their position on contour in the complex time plane.[45] It is important to note that equations must first be solved in the complex time domain, and then analytically continued to the real axis. The analytic continuation is performed before the Fourier transform, so we must be careful about how we deal with the Fourier transformed equations. Here we discuss the equations of motion satisfied by the Fourier transforms of the time-ordered Green's functions, and only summarize the rules for analytic continuation at the end of this appendix. All Green's functions and self-energies in the following expressions are function of frequency ω, and, therefore, we omit their argument to simplify the notation.

The Green's function for the impurity state G_a can be written in a standard way,

$$G_a = (\omega - \epsilon_0 - \Sigma_a)^{-1}, \tag{A2}$$

using the self-energy $\Sigma_a(\mathbf{R}_t, Z_0; \omega)$. The solution for G_a is thus reduced to finding Σ_a. We first treat a closed-shell or a nonmagnetic open-shell ($V_{ka} \gg U$) adsorbate for which electron correlations can be neglected. We begin by considering the tip-substrate system without the adsorbate. We define $\tilde{G}_{kk'}$ and $\tilde{G}_{pp'}$ in analogy with G_a [Eq. (A1)] as the Green's functions of the metal and tip states, respectively, in the absence of the adsorbate. These are not identical with the Green's functions $G_{kk'}$ and $G_{pp'}$ for the full system introduced in Appendix B. The bare metal-tip system is described by the Hamiltonian of Sec. II with $\epsilon_0 = U = t_{ap} = V_{ak} \equiv 0$. Using the equations of motion, we can write

$$(\omega - \epsilon_k)\tilde{G}_{kk'} = \delta_{kk'} + \sum_{k''} \Sigma_{kk''}\tilde{G}_{k''k'} \tag{A3}$$

and

$$(\omega - \epsilon_p)\tilde{G}_{pp'} = \delta_{pp'} + \sum_{p''} \Sigma_{pp''}\tilde{G}_{p''p'} \tag{A4}$$

where the self-energies are $\Sigma_{kk'} = \Sigma_p t_{kp} G_p^0 t_{pk'}$ and $\Sigma_{pp'} = \Sigma_k t_{pk} G_k^0 t_{kp'}$ and $G_k^0 = (\omega - \epsilon_k + i\eta_k)^{-1}$ and $G_p^0 = (\omega - \epsilon_p + i\eta_p)^{-1}$ are the Green's functions for the clean metal and tip, respectively, without their mutual interaction. The solutions for $\tilde{G}_{kk'}$ and $\tilde{G}_{pp'}$ can be formally written as the inverse of $D_{kk'} = \delta_{kk'}(\omega - \epsilon_k) - \Sigma_{kk'}$ and $D_{pp'} = \delta_{pp'}(\omega - \epsilon_p) - \Sigma_{pp'}$. We also define the adsorbate-metal and adsorbate-tip hybridization matrices modified by the tip-substrate interaction as $\tilde{V}_{ka} = V_{ka} + \Sigma_p t_{kp} G_p^0 t_{pa}$ and $\tilde{t}_{pa} = t_{pa} + \Sigma_k t_{pk} G_k^0 V_{ka}$. With these definitions and with $\tilde{G}_{kk'}$ and $\tilde{G}_{pp'}$ obtained through Eqs. (A3) and (A4), the solution for the noninteracting Σ_a is formally given by

$$\Sigma_a = \sum_{kk'} V_{ak}\tilde{G}_{kk'}\tilde{V}_{k'a} + \sum_{pp'} t_{ap}\tilde{G}_{pp'}\tilde{t}_{p'a}. \tag{A5}$$

The evolution of the self-energy Σ_a is rather complicated in the general case of strong tip-to-substrate coupling. We proceed with formulation of the general nonequilibrium theory for the tunneling current using this self energy (Sec. III A) and then we discuss two limiting cases: (a) the equilibrium limit $|t_{kp}|, |t_{ap}| \ll |V_{ka}|$ (Sec. III B) in which case the second term in Eq. (A5) is neglected, and $\tilde{V}_{ka}$ and $\tilde{G}_{kk'}$ are replaced by V_{ka} and $G_k^0\delta_{kk'}$; and (b) the nonequilibrium case under the assumption $|t_{kp}| \ll |t_{ap}| \sim |V_{ka}|$, in which case we keep both terms in Eq. (A5) and replace $\tilde{V}_{ka}$, $\tilde{t}_{ap}$, $\tilde{G}_{kk'}$, and $\tilde{G}_{pp'}$ by V_{ka}, t_{ap}, $G_k^0\delta_{kk'}$, and $G_p^0\delta_{pp'}$. Section IV B 3 deals with tunneling through a Kondo impurity in this limit. Case (b) includes the effect of the increased hybridization of the discrete state due to the tip presence and the onset of nonequilibrium population on the adsorbate at finite bias.

In order to study these corrections in limit (b), ($|t_{pk}| \ll |t_{pa}| \sim |V_{ka}|$), we replace the Green's functions $\tilde{G}_{kk'}$ and $\tilde{G}_{pp'}$ by the noninteracting ones, i.e., $\tilde{G}_{kk'} = \delta_{kk'}G_k^0$ and $\tilde{G}_{pp'} = \delta_{pp'}G_p^0$ and the modified $\tilde{V}_{ka}$ and $\tilde{t}_{pa}$ by V_{ka} and t_{pa}. The self-energy Σ_a then simplifies to

$$\Sigma_a^0 = \sum_k |V_{ak}|^2 G_k^0 + \sum_p |t_{ap}|^2 G_p^0. \tag{A6}$$

The largest source of error in writing the approximate self energy is the neglect of the possibly significant interference effects at larger t_{kp} as a result of the phase difference between $\tilde{t}_{pa}$ and t_{pa}. It is always reasonable to replace $\tilde{V}_{ka}$ by V_{ka}, as long as the adsorbate is on the surface rather than on the STM tip. This general case will be the topic of a future study. If the tip distance from the adsorbate is much larger than the adsorbate-metal separation, so that $t_{ap} \ll V_{ak}$, the self-energy is well described by the first term only. In such a

case, the STM does not strongly modify the studied system. It is then reasonable to characterize the system without the presence of the STM tip, and then consider the tunneling.

Finally, we discuss the Green's function G_a in limit (b) for a Kondo impurity which is likely to show stronger dependence on the bias and tip interaction. We find the nonequilibrium Green's function G_a under the same assumption that lead to Σ_a^0 for the noninteracting Anderson Hamiltonian. We solve the interacting system in the limit of $U=\infty$ using the NCA approximation. The self-energy is not a simple sum of the two contributions from the metal and tip as it was the case in the noninteracting system, because the occupation of the resonance is limited to one electron and the hybridization is now correlated—formally through the slave boson Green's function $B(\omega)$. The two coupled equations are solved self-consistently.

APPENDIX B: EQUATIONS OF MOTION FOR G_{pk} AND G_{pa}

In this appendix, we find the solution for $(\Sigma_{kp}t_{kp}G_{pk}+\Sigma_{ap}t_{ap}G_{pa})$ entering the expression for the tunneling current [Eq. (3.3)] for the general case of arbitrary tip-system coupling. Ultimately, the interesting regime in connection with typical STM experiments is one in which $t_{kp},t_{ap}<V_{ak}$. However, we want to be able, in principle, to study the system when the coupling of the STM tip to the system and the tunneling current are strong. This creates nonequilibrium occupation on the adsorbate resonance and modifies the spectroscopic properties of the system. We therefore proceed by deriving the most general expression valid for arbitrary coupling strength t_{kp} and t_{ap}, and discuss an approximation (b) that allows us to take into account the most important nonequilibrium effects as described in Appendix A. For this purpose we introduce the Green's function $G_{pa}(\omega)$, $G_{pk}(\omega)$, $G_{kk'}(\omega)$, $G_{pp'}(\omega)$, and $G_{ka}(\omega)$ as the Fourier transform of

$$G_{ij}(t,t')=-i\langle T_C c_i(t)c_j^\dagger(t')\rangle. \tag{B1}$$

We now turn to the equations of motion for the Green's functions relevant for the tunneling current. The following expressions are valid for arbitrary interaction $U\neq 0$, and the nature of the intra-adsorbate interactions are contained fully in the solution for G_a discussed in Appendix A. The first term in the current [Eq. (3.3)] contains the tip-adsorbate propagator which satisfies

$$(\omega-\epsilon_p)G_{pa}=t_{pa}G_a+\sum_k t_{pk}G_{ka}. \tag{B2}$$

This is expressed in terms of G_a, already solved within a given approximation in Appendix A through Eq. (A2), and in terms of the metal-adsorbate Green's function

$$(\omega-\epsilon_k)G_{ka}=V_{ka}G_a+\sum_p t_{kp}G_{pa}. \tag{B3}$$

The last two equations are coupled and need to be solved self-consistently. We do this by substituting Eq. (B3) for G_{ka} in Eq. (B2), and vice versa. The solutions are then expressed in terms of G_a, $\tilde{G}_{pp'}$, and $\tilde{t}_{pa}$ discussed in Appendix A as

$$G_{pa}=\sum_{p'}\tilde{G}_{pp'}\tilde{t}_{p'a}G_a. \tag{B4}$$

We will also need the solution for G_{ak}. The tip-induced correction to V_{ka} contributes to the phase of V_{ka}, as well as its magnitude, and could thus affect the line shape significantly in the strong-coupling limit. But it should be particularly weak when $t_{kp},t_{pa}\ll V_{ka}$, and it will be safe to ignore it. We write

$$G_{ak}=G_a\sum_{k'}\tilde{V}_{ak'}\tilde{G}_{k'k}. \tag{B5}$$

The second term in Eq. (B3) is negligible when the tip-adsorbate separation is much larger than the adsorbate-metal separation. Neglecting this term is equivalent to replacing $\tilde{G}_{pp'}\rightarrow G_p^0\delta_{pp'}$ in Eq. (B4) and $\tilde{G}_{kk'}\rightarrow G_k^0\delta_{kk'}$ and $V_{ka}\rightarrow V_{ka}$ in Eq. (B5). The tip-adsorbate Green's function G_{pa} is then expressed entirely in terms of G_a and the unperturbed conduction electron Green's functions.

The second term in Eq. (3.3) contains the tip-metal propagator G_{pk}, which satisfies

$$(\omega-\epsilon_p)G_{pk}=\sum_a t_{pa}G_{ak}+\sum_{k'}t_{pk'}G_{k'k}. \tag{B6}$$

It is expressed in terms of G_{ak} [Eq. (B5)] discussed in the previous paragraph, and in terms of $G_{k'k}$, the Green's function for the substrate conduction electrons

$$(\omega-\epsilon_{k'})G_{k'k}=\delta_{kk'}+\sum_a V_{k'a}G_{ak}+\sum_p t_{k'p}G_{pk}. \tag{B7}$$

We see that $G_{kk'}$ couples to G_{pk} [Eq. (B6)], and also to G_{ak} [Eq. (B5)], already solved in terms of G_a and $\tilde{G}_{kk'}$. The last two equations can be solved self-consistently to give

$$G_{k'k}=\tilde{G}_{k'k}+\sum_{k_1k_2}\tilde{G}_{k'k_1}\tilde{V}_{ak_1}G_a\tilde{V}_{k_2a}\tilde{G}_{k_2k} \tag{B8}$$

and

$$G_{pk}=\sum_{p'}\tilde{G}_{pp'}\left(t_{p'k}+\sum_{ak'}\tilde{t}_{p'a}G_a\tilde{V}_{ak_1}\right)G_k^0. \tag{B9}$$

For the purpose of analytic continuation, it is important to keep track of the order in which the Green's functions appear in the product in the above equations. The equilibrium limit of the theory is achieved by neglecting the last term in Eq. (B7) along with the equivalent approximations for G_a and G_{ak} discussed above. This removes the self-consistency requirement and neglects the effect of the tip on the substrate conduction electrons, but not on the tunneling current. The solution for $G_{kk'}$ is then identical to that of the system without the tip.

The rules for writing the expression for the ''lesser'' and retarded functions in the frequency space can be summarized as follows.[44–46,26] If the time-ordered Green's function $A(\omega)$ is given in terms of the product of propagators,

$$A(\omega)=B(\omega)\cdots Z(\omega); \tag{B10}$$

then

$$A^{R(A)}=B^{R(A)}\cdots Z^{R(A)} \tag{B11}$$

and

$$A^{\gtrless}=\cdots+B^{R}\cdots C^{\gtrless}\cdots Z^{A}+\cdots. \tag{B12}$$

We refer the reader to Haug and Jauho[46] for details.

[1] *Tunneling Phenomena in Solids*, edited by E. Burstein and S. Lundqvist (Plenum, New York, 1969).
[2] C. B. Duke, *Tunneling in Solids* (Academic, New York, 1969).
[3] E. L. Wolf, *Principles of Electron Tunneling Spectroscopy* (Oxford University Press, New York, 1985).
[4] L. Esaki, I. Giaver, and B. D. Josephson, in *Nobel Lectures in Physics 1971–1980*, edited by S. Lundqvist (World Scientific, Singapore, 1992), pp. 109–164.
[5] R. Young, J. Ward, and F. Scire, Rev. Sci. Instrum. **43**, 999 (1972).
[6] G. Binnig and H. Rohrer, Rev. Mod. Phys. **59**, 615 (1987).
[7] *Scanning Tunneling Microscopy*, Methods of Experimental Physics, Vol. 27, edited by J. A. Stroscio and W. J. Kaiser (Academic, San Diego, 1993).
[8] *Scanning Tunneling Microscopy III: Theory of STM and Related Scanning Probe Methods*, edited by R. Wiesendanger and H.-J. Güntherodt (Springer-Verlag, Berlin, 1993).
[9] R. Wiesendanger, *Scanning Probe Microscopy and Spectroscopy* (Cambridge University Press, Cambridge, 1994).
[10] C. J. Chen, *Introduction to Scanning Tunneling Microscopy* (Springer, Berlin, 1996).
[11] J. Kondo, Prog. Theor. Phys. **32**, 37 (1964).
[12] J. Kondo, Solid State Phys. **23**, 183 (1969).
[13] A. C. Hewson, *The Kondo Problem to Heavy Fermions* (Cambridge University Press, Cambridge, 1993).
[14] J. A. Appelbaum, J. C. Phillips, and G. Tzouras, Phys. Rev. **160**, 554 (1967).
[15] C. B. Duke and M. E. Alferieff, J. Chem. Phys. **46**, 923 (1967).
[16] E. W. Plummer, J. W. Gadzuk, and R. D. Young, Solid State Commun. **7**, 487 (1969).
[17] J. W. Gadzuk and E. W. Plummer, Rev. Mod. Phys. **45**, 487 (1973).
[18] J. W. Gadzuk, Phys. Rev. B **47**, 12 832 (1993).
[19] *Single Charge Tunneling: Coulomb Blockade Phenomena in Nanostructures*, edited by H. Grabert and M. H. Devoret (Plenum, New York, 1992).
[20] D. Goldhaber-Gordon, H. Shtrikman, D. Mahalu, D. Abusch-Magder, U. Meirav, and M. A. Kastner, Nature (London) **391**, 156 (1998).
[21] V. Madhavan, W. Chen, T. Jamneala, M. F. Crommie, and N. S. Wingreen, Science **280**, 567 (1998).
[22] J. Li, W. D. Schneider, R. Berndt, and B. Delley, Phys. Rev. Lett. **80**, 2893 (1998).
[23] J. Bardeen, Phys. Rev. Lett. **2**, 57 (1961).
[24] J. Tersoff and D. R. Hamann, Phys. Rev. B **31**, 805 (1985).
[25] S. Gao, M. Persson, and B. I. Lundqvist, Phys. Rev. B **55**, 4825 (1997).
[26] G. D. Mahan, *Many-Particle Physics* (Plenum, New York, 1990).
[27] G. F. Koster and J. C. Slater, Phys. Rev. **96**, 1208 (1954).
[28] P. W. Anderson, Phys. Rev. **124**, 41 (1961).
[29] U. Fano, Phys. Rev. **124**, 1866 (1961).
[30] C. Cohen-Tannoudji, J. Dupont-Roc, and G. Grynberg, *Atom-Photon Interactions* (Wiley, New York, 1992).
[31] D. Penn, R. Gomer, and M. H. Cohen, Phys. Rev. B **5**, 768 (1972).
[32] C. J. Chen, Phys. Rev. Lett. **65**, 448 (1990).
[33] C. J. Chen, J. Vac. Sci. Technol. A **9**, 44 (1991).
[34] N. D. Lang, A. Yacoby, and Y. Imry, Phys. Rev. Lett. **63**, 1499 (1989).
[35] U. Wille, Phys. Rev. B **50**, 1888 (1994).
[36] J. W. Gadzuk, Surf. Sci. **6**, 133 (1967).
[37] P. Nordlander and J. C. Tully, Phys. Rev. B **42**, 5564 (1990).
[38] A. G. Borisov, R. Zimny, D. Teillet-Billy, and J. P. Gauyacq, Phys. Rev. A **53**, 2457 (1996).
[39] P. Sautet, Surf. Sci. **374**, 406 (1997).
[40] M. Plihal, D. C. Langreth, and P. A. Nordlander, Phys. Rev. B **59**, 13 322 (1999).
[41] H. Eyring, J. Walter, and G. E. Kimball, *Quantum Chemistry* (Wiley, New York, 1944).
[42] I. N. Levine, *Quantum Chemistry*, 5th ed (Prentice Hall, Englewood Cliffs, NJ, 2000).
[43] L. V. Keldysh, J. Eksp. Teor. Fiz. **47**, 1515 (1964) [Sov. Phys. JETP **20**, 1018 (1965)].
[44] L. P. Kadanoff and G. Baym, *Quantum Statistical Mechanics* (Benjamin, New York, 1962).
[45] D. C. Langreth, in *Linear and Nonlinear Electron Transport in Solids*, edited by J. T. Devreese and V. E. van Doren (Plenum, New York, 1976).
[46] H. Haug and A.-P. Jauho, *Quantum Kinetics in Transport and Optics of Semiconductors* (Springer, Berlin, 1996).
[47] M. Plihal and D. C. Langreth, Phys. Rev. B **58**, 2191 (1998).
[48] T. Kawasaka and H. K. A. Okiji, Phys. Lett. A **250**, 403 (1998).
[49] T. Kawasaka, H. Kasai, W. A. Dino, and A. Okiji, J. Appl. Phys. **86**, 6970 (1999).
[50] N. S. Wingreen and Y. Meir, Phys. Rev. B **49**, 11 040 (1994).
[51] N. Sivan and N. S. Wingreen, Phys. Rev. B **54**, 11 622 (1996).
[52] E. W. Plummer and W. Eberhardt, Adv. Chem. Phys. **49**, 533 (1982).
[53] S. D. Kevan and R. H. Gaylord, Phys. Rev. B **36**, 5809 (1987).
[54] J. W. Gadzuk, J. Vac. Sci. Technol. **9**, 591 (1972).
[55] S. D. Kevan and R. H. Gaylord, Phys. Rev. Lett. **57**, 2975 (1986).
[56] M. P. Everson and R. C. Jaklevic, J. Vac. Sci. Technol **8**, 3662 (1990).

[57] W. Chen, V. Madhavan, T. Jamneala, and M. F. Crommie, Phys. Rev. Lett. **80**, 1469 (1998).
[58] M. F. Crommie, C. P. Lutz, and D. M. Eigler, Science **262**, 218 (1993).
[59] M. F. Crommie, C. P. Lutz, D. M. Eigler, and E. J. Heller, Physica D **83**, 98 (1995).
[60] L. Bürgi, O. Jeandupeux, H. Brune, and K. Kern, Phys. Rev. Lett. **82**, 4516 (1999).
[61] Y. Hasegawa and P. Avouris, Phys. Rev. Lett. **71**, 1993 (1993).
[62] P. Avouris, I.-W. Lyo, and P. Molinas-Mata, Chem. Phys. Lett. **240**, 423 (1995).
[63] H. C. Manoharan, C. P. Lutz, and D. M. Eigler, Nature (London) **403**, 512 (2000).
[64] A. Schiller and S. Hershfield, Phys. Rev. B **61**, 9036 (2000).
[65] P. Coleman, Phys. Rev. B **29**, 3035 (1984).
[66] N. D. Lang, Phys. Rev. Lett. **58**, 45 (1987).
[67] T. Jamneala, V. Madhavan, W. Chen, and M. F. Crommie, Phys. Rev. B **61**, 9990 (2000).
[68] M. Plihal, D. C. Langreth, and P. A. Nordlander, Phys. Rev. B **61**, 13 341 (2000).
[69] O. Újsághy, J. Kroha, L. Szunyogh, and A. Zawadowski, Phys. Rev. Lett. **85**, 2557 (2000).